Research Square

Preprints are preliminary reports that have not undergone peer review.
They should not be considered conclusive, used to inform clinical practice,
or referenced by the media as validated information.

H∞-dCNN: Enhancing the SNR using Deep Learning Algorithm in Wireless Communication System

C. Priya
Karpagam College of Engineering
D. Kumutha (skvijaykumu@gmail.com)
SJB Institute of Technology
M. Shilpa
M S Ramaiah Institute of Technology
K. Jayanthi
Government Engineering College
S. Baskaran
S.K.P. Engineering College

Research Article

Keywords: Wireless Communication, Deep Learning, Optimization, Quality of Service, Convolution Neural Network, Hybrid Infinity Bit Error Rate

Posted Date: May 17th, 2021

DOI: https://doi.org/10.21203/rs.3.rs-491094/v1

License: This work is licensed under a Creative Commons Attribution 4.0 International License.
Read Full License

H_∞-dCNN: Enhancing the SNR using Deep Learning Algorithm in Wireless Communication System

[1]C.Priya, Associate Professor, Karpagam College of Engineering, coimbatore

[2]D. Kumutha, Assistant Professor, SJBIT, Bangalore
[3]M.Shilpa, Associate ProfessorM S Ramaiah Institute of Technology, Bangalore
[4]K.Jayanthi, Assistant Professor, Government Engineering College, Salem
[5]S.Baskaran, Professor, S.K.P Engineering College, Thiruvannamalai

[1]priyakarthikayeni@gmail.com, [2]skvijaykumu@gmail.com, [3]mallikashilpa@gmail.com, [4]jayanthikathir4413@gmail.com, [5] skpbaskar@gmail.com

Abstract

In Wireless communication systems, the deep learning-based Convolution Neural Networks (dCNN) is performed to gain a better improvement of Quality of Services(QoS) with higher Signal to Noise Ratio (SNR). Multiple Input and Multiple Output (MIMO) systems are presented for real-time evaluation from various technologies, which has served the purpose of services in improving the communication performance of the physical layer of the wireless network. By increasing the communication throughput by focusing on resource allocation, the overall efficiency was not up to the market due to the network's dynamic behavior. This article proposes the system in two different stages to express the analytical solution for decreasing the Bit Error Rate(BER). The first is to employ the Hybrid Infinity (H_∞) through the channel for better robustness in wireless network computing. Next is to optimize Bit Error Rate (BER) with carrier detection as well as other criteria for improving service quality by analyzing the network behavior using Deep Learning Algorithm. The deep Convolution Neural Network with Hybrid Infinity (H_∞ - dCNN) is implemented and evaluates the low BER values with high SNR for the performance of QoS. Thus, H_∞ - dCNN is proved and outperform the simulated results with better characteristics by using the Matlab software. Hence, the mathematical expression for the proposed system is noticed that a significant improvement is obtained in terms of BER lesser than $0.6\,e^{-4}$. It is observed the SNR lesser than 18dB, which is comparatively best than the baseline method.

Keywords: Wireless Communication, Deep Learning, Optimization, Quality of Service, Convolution Neural Network, Hybrid Infinity Bit Error Rate.

1. Introduction

Wireless communication can be assumed to be the backbone for any kind of advanced communication systems developed in recent days. It must be said that the advancement in smart devices has significantly been boosted by the advancement in wireless communication. Multiple Input and Multiple Output (MIMO) is a means, it multiplies and enhances the capacity of radio links using several antennas for transmission and reception. MIMO predominantly exploits the feature of multipath propagation. MIMO deploys smart transmitters and receivers to increase the range and speed of transmission. According to MIMO, wireless systems can be considered as an extension to smart antennas [1] [2] [3]. The primary benefits of MIMO technology are that multiple antenna configurations are deployed to overcome the null effect of multi-path propagation and fading. Also, MIMO provides superior data range, data rates, and reliability.

Orthogonal Frequency Division Multiplexing (OFDM) is a typically used digital signaling technique for encoding digital data across inter-carrier channels. OFDM provides great benefits for data links. OFDM is predominantly the most commonly used multiplexing technique across wideband communication and high-speed wireless networks. OFDM can be considered as an example of multicarrier modulation. Figure.1 explains the working of OFDM. OFDM can be assumed as a cluster of demodulators that translates each carrier. During the symbolic period, the corresponding signal is combined to regenerate the carriers ' data [4] [5] [6]. The primary requirement of an OFDM transmitting and receiving systems is that the carriers must be linear. Any discrepancy in meeting this requirement will result in interference of carrier frequencies and will create distortion.

In general, the radio signals transmit the data one bit after another in a serial fashion. But with OFDM, the data is transmitted in parallel by using multiple carriers. The salient features of OFDM are multiple carriers which carry parallel data. Also, these carriers are orthogonal to each other. A guard signal is introduced to avoid inter-symbol interference and minimize channel delays. The primary benefits of OFDM are that OFDM is highly resilient to selective fading and interference. OFDM is also highly robust to inter-symbol interference. The primary disadvantages of OFDM are that it is extremely sensitive to the carrier and offset drift and sometimes suffers from increased peak to average power ratio. Nowadays MIMO and OFDM are used in conjunction to minimize inter-symbol interference [7]. Along with the

coupling of MIMO and OFDM, deep learning-based Convolution Neural Networks (dCNN) are deployed to enhance the quality of service in wireless communication systems.

Antenna design is important because the frequency between antennas does not suit and contributes to a decline in efficiency when various antennas with distinct frequencies are positioned tightly. Many models, but with complicated constructions, have appeared in the latest days. The antennas should have a simple framework with a smaller size, to produce strong isolation at several frequencies. The proposed system concentrates on the development of a novel MIMO multiband antenna for emerging wireless systems.

2. Literature Review

Over the last decade, machine learning and its successors such as CNN and Deep learning have been seen as a potential candidate for performing supervised classification across several domains such as networking, image processing, etc. Initially, machine learning was seen as a successful classification approach to address small problems. The term “Deep” is associated with the neural network to signify the use of advanced and sophisticated layers that run deep. As suggested in [8], deep learning approaches are highly robust when compared to shallow supervised approaches. Also, deep convolution neural network-based architectures are predominantly driven by iterative algorithms [9]. Recent trends have seen the deployment of deep learning approaches for enhancing the decoder performance across linear channels [10]. Also, several works [11 - 14] have been carried out to learn how to invert and work with linear channels and at the same time reconstruct signals that have been developed.

Authors of [3] have proposed an artificial and parallel bee colony (P-ABC) based parallel approach. The performance of this approach was measured in terms of the ratio of peak and average power and the reduction in PAPR has been cited. Author in [15] improved channel estimation output using an ILSA (Iterative Least Square) algorithm in MIMO-OFDM applications. An analog feedback system based on time-domain compression for MIMO-OFDM and it has been proposed in [16]. Whereas it is proposed to increase the feedback-quality and deal with the problem in differentiating more signals. A training sequence has been designed to perform channel estimation in the communication systems, which has been analyzed in [17] and the necessary criteria for a training sequence have been identified to minimize MSE. A subcarrier-based grouping algorithm has been designed and proposed in [18] for reducing the feedback load in the case of a multi-antenna downlink system with

OFDM. This proposed method chooses a quantization vector and the highest sum rate than the other conventional algorithms. Authors of [19] have proposed a new phase offset SLM Scheme that is focussed on PAPR reduction when applied across MIMO-OFDM systems without any additional information [21] [22]. Authors of [20] have explored the feasibility of how spectrum sharing can be utilized among radar systems and wireless communication systems. Both systems comprise of BS of full-duplex for serving users in uplink and downlink under the same frequency and time. Authors of [23] have developed and discussed the architecture behind an FD-MIMO. A hybrid and asymmetrical optical OFDM (AHO-OFDM) approach for diminishing vision light communication systems have been proposed in [24].

For mobile telephones, a tiny volume compact and wideband MIMO antenna were suggested [25]. For most LTE, WiMAX, and WLAN frequencies of 1.79–3.77 GHz, the transmitter was relevant. The antenna geometry was intended to achieve excellent insulation between the entry channels by using two symmetric radiating components with four divisions and a T-shaped parasite component. Simulation examined the efficiency of the antenna and then measured it. The tested antenna radiation pattern was almost all-oriented and demonstrates an excellent chance of profit. Also, there seem to be great ECC scores for the antenna components. Therefore, a MIMO antenna was designed in this study.

The main structure of the antenna suggested was relied therefore on two events of leaking waves: one happens on the matrix of the substrate while the other happens on the pit that is integrated into the substrate of high permittivity [26]. For applications of the K-band, they have developed a completely integrated Fabry-Perot tube antenna. At a resonance frequency of 21,6 GHz, a known impedance bandwidth of over 8 percent and 3 dB gained bandwidth of about 1.3 percent. The peak increase at the resonance frequency was around 13.1 dBi, which suggests that the leaky-wave dipole dipped stimulated the resonance of the body of the substratum. Furthermore, the antenna seems to be poor-profile, simple to integrate into circuit boards, mechanical robustness, and great cost-effectiveness.

It can be understood from the above works the significance and need for deploying MIMO-OFDM across communication channels. Also, these works signify the importance of deep convolution neural networks across these communication channels to enhance the quality of service parameters.

2.1 Limitations

Deep convolution neural networks have been considered as one of the most prominent means for performing supervised classification. However, dCNN has got its limitations and challenges lying ahead. Deep learning requires large volumes of data for training and also the presence of several hidden layers increases the development complexity. When it comes to transparency of output, it is very difficult to demonstrate how and what were the data transitions that evolved while arriving at a particular output. Deep learning is known to be a resource-intensive concept. This involves deployment of more powerful GPUs with high processing capabilities, large volumes of storage areas to train the models, etc. Also, Deep Learning requires a larger time to train when compared with conventional machine learning.

2.2 Motivation

As observed from the literature review, it can be said that MIMO combined with OFDM has been the predominant modulation technique that is deployed across wireless communication channels in recent years. However, the MIMO-OFDM based system needs to ensure perfect carrier selection and efficient resource and bandwidth utilization. This, in turn, will enhance the Quality of Service aspects of MIMO-OFDM communication. It has been proved that using deep convolution neural networks for analyzing the input data stream can provide better resource allocation, carrier sensing, and optimizing the other requirements and subsequently enhance several QoS parameters that are instrumental in determining the efficient functioning of the MIMO-OFDM system. The proposed system concentrates on the model of a novel MIMO multiband antenna for emerging wireless systems.

2.3 Existing System

In the existing system [13] [27], the author used deep learning algorithms for optimizing the coverage and capacity of the network. In the existing approach, optimal user selection, scheduling, average channel gain factor calculation, and signal strength for communication. Along with this, capacity-coverage, intercell interference coordination are verified before scheduling to the user. The existing system focused on group-users and the external behavior supporting MIMO communication. But our proposed work focused on optimizing the internal network behavior in the MIMO network. And it is trusted that, if the internal behavior of the network is optimized then, it automatically strengthens and improves the communication throughput. In this paper, the basis deep learning function on the physical layer of the MIMO network is referred to from [32] [33] [35].

3. Proposed Approach

3.1 Structure of antenna and process of decoupling

Figure.1 demonstrates the multiband antenna system of MIMO with a 40 / 40 mm2 FR4 substratum with 1.6 mm density and is symmetrically positioned on it by the two three-band monopolies. The system consists of a T-shaped monopoly straight aroused from the floor by the 50-TAPmicrostrip line, which generates more than 4 GHz range. The two reversed L tubes are combined with the Monopoly in the form of a T. Stubs A and B have been arranged for 3.5 and 6.9 GHz resonance on both sides of the T-shape monopoly and have been used. At the respective frequency, the optimum duration of the resonant structures corresponds around a quarter-wave longitude. Figure.2(a & b) models a tri-band monopoly S11 displayed and adjusting the geometric and locations attributes of two inverted-L-stubs enhances the corresponding impedance feature.

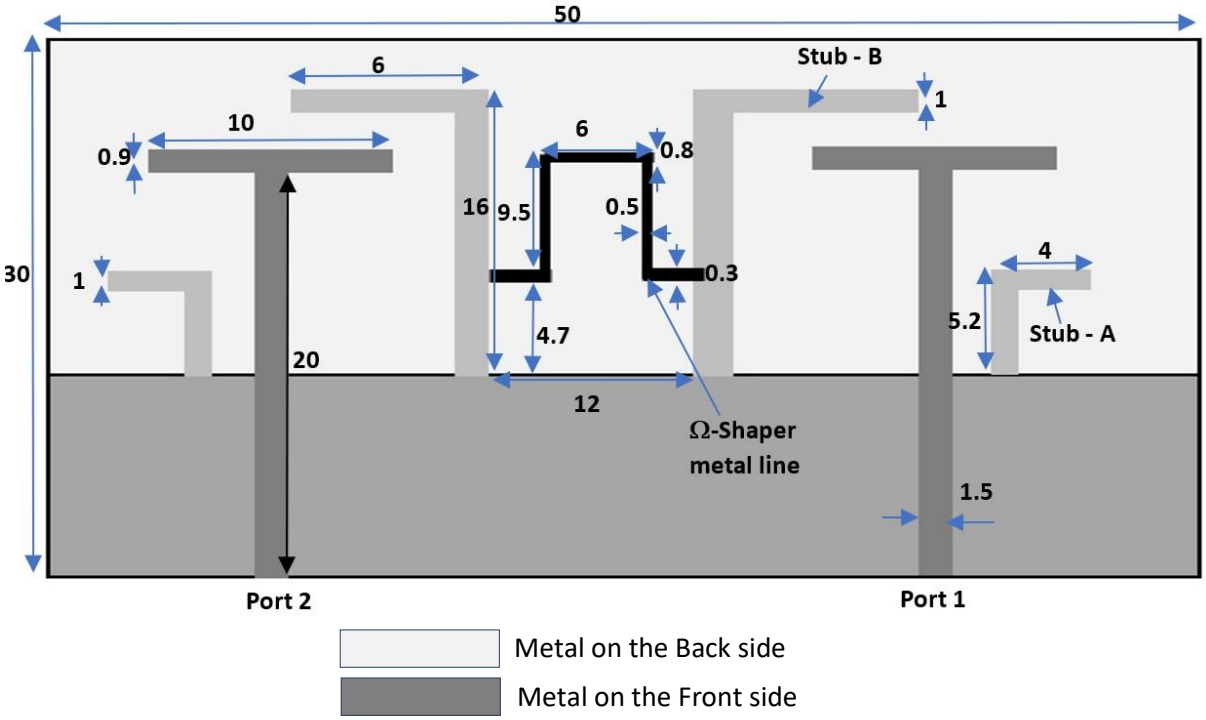

Figure. 1. Multiple Antenna System

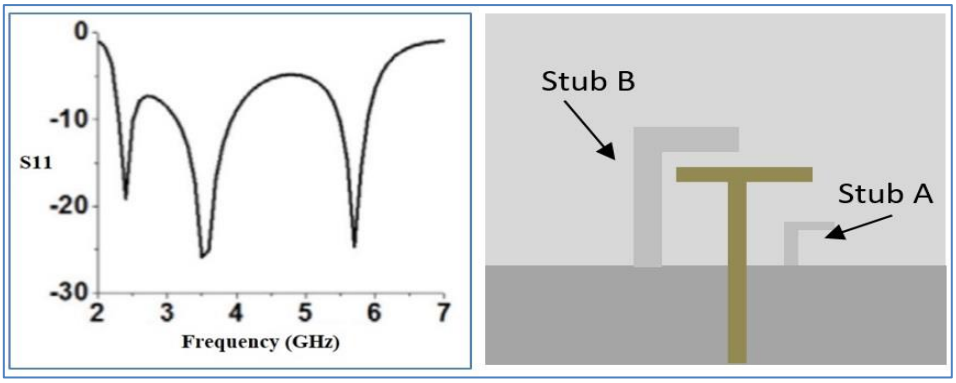

Figure. 2. (a). Triband Monopole(S11) **Figure. 2. (b). Triband Monopole**

Both monopolies are used without any additional disconnecting instruments to create a MIMO antenna (marked MIMO I). The closer inverted-L stubs are close to the MIMO I center, and the smaller stubs are on both ends. Figure.3 displays MIMO I composition and S-parameters. The impedance of the two entry channels is equal because of the symmetrical arrangement. Only S11 and S12 are displayed for simplicity. The MIMO antenna has excellent functioning in terms of impedances and decoupling characteristics on both higher strips more than 3.8 and 6.8GHz. The B stub can also decrease the interconnected connection for both greater channels. However, the elevated shared bonding deteriorates the impedance at the low band. To fix this issue, a metal string in the shape of an antenna has been produced to connect two larger stubs (designated Bs) to neutralize the connection of the antenna to the antenna by incorporating a current new route between them. In Figure. 3, the tap shaped panel of the MIMO (marked MIMO II) is demonstrated, along with its related S-parameters displayed. The shared couple of 3.4 GHz is reduced from-16 dB to -32dB, as shown by the introduction of the iron-shaped row. The S11 has been enhanced from -14 dB to-42 dB, thanks to the suppression of decay of the corresponding impedances induced by shared bonding. Furthermore, in the greater frequency ranges, the tap shaped string, physically linked to the two 3.4 GHz resonators, has little impact on S11. Because three resonators are installed on the tri-band monopoly for three frequencies, the inclusion of a "t" row only affects the efficiency of stub B. Also, the S21 variety is appropriate. Thus, the re-optimization of additional resonators is not necessary if the tap shaped string is inserted. The MIMO II tri-band antenna suggested as MIMO.

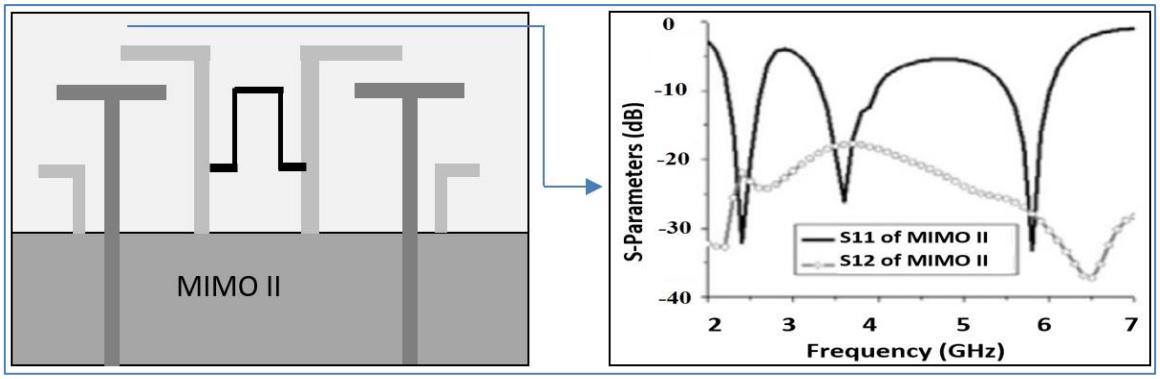

Figure. 3(a) Symbol of MIMO II **Figure. 3(b)** MIMO II's S-parameters

3.2 Deep Learning-Based MIMO Communications

This section focused on various factors of the MIMO system and applied in dCNN for learning and predicting the best path automatically.

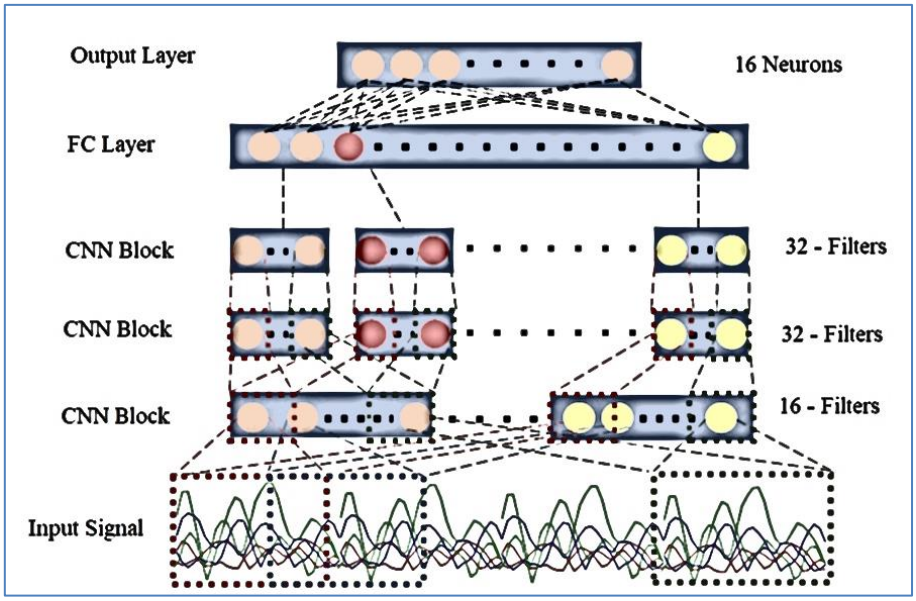

Figure-4. Basic Deep Learning Structure

The structure of the proposed deep CNN model is given in Figure-4. It has an input and one output layer. N number of CNN layer with one fully connected layer is available between the input and FC layer. It is the designer's convenient to involve any number of fully connected layers, and it is depending on the number of classes classified. In this architecture, the pooling layer is used with CNN to increase the performance. The set of all factors considered in the MIMO system with deep learning is described below.

3.2.1 Spatial Diversity

In MIMO several spatial or space diversity methods are used for enhancing the recital of the wireless link in terms of reliability, coverage, and robustness. One of the techniques is STBC coding used in $\mathbf{2} \times \mathbf{1}$ MIMO system discussed in Alamouti (1998), and it is called as Alamouti Coding (AC). AC provides equal performance to MRRC (Maximal Ratio Receiver Combining) method while the power of $\boldsymbol{T_X}$ is doubled. Using this method, within a defined symbol-period two symbols $\boldsymbol{s_1}$ and $\boldsymbol{s_2}$ are transferred from first and second antennas respectively. At the time of next symbol-period, $-\boldsymbol{s_2^*}$ and $\boldsymbol{s_1^*}$ are transmitted from the first and second antenna respectively where * indicates the complex conjugate form. From this, it is very clear that there is no improvement in the network throughput and it needs two more time slots for transmitting the two symbols. The signals received at the receiver antenna ports 1, 2 is represented as:

$$R_1 = H_1 s_1 + H_2 s_2 + N_1 \qquad (1)$$

$$R_2 = -H_1 s_2^* + H_2 s_1^* + N_1 \qquad (2)$$

Where the channel variables are represented as $\boldsymbol{H_1}$ and $\boldsymbol{H}$, and $\boldsymbol{N_1}$, and $\boldsymbol{N_2}$ represents the noise in equation (1 & 2). Both the channel and noise variables are involved with circularly symmetric complex gaussian entries with zero-means. Finally, the symbols $\boldsymbol{s_1}$ and $\boldsymbol{s_2}$ are estimated using the MMSE (Minimum Mean Square Error) parameter. The STBC coding method used in $\mathbf{2} \times \mathbf{1}$ MIMO is created to have N- $\boldsymbol{T_X}$ and M- $\boldsymbol{R_X}$ antennas, which are discussed in V. Tarokh et al. (1998). Hence, this paper focused on evaluating the performance of $\mathbf{2} \times \mathbf{1}$ MIMO system.

3.2.2 Spatial Multiplexing

In MIMO, user throughput is increased using the spatial multiplexing method already used in E. Telatar (1999), W. Yu et al. (2004). Let consider N number of $\boldsymbol{T_X}$ and $\boldsymbol{R_X}$ antennas are available in the MIMO single-user system. Then the number of symbols transmitted in $\boldsymbol{T_X}$ is $\boldsymbol{M_t} \times 1$, and the received signal at $\boldsymbol{R_X}$ is $\boldsymbol{y = Hs + N}$ (where $H = \boldsymbol{M_r} \times \boldsymbol{M_t}$, is the channel matrix) where s is $\boldsymbol{M} \times 1$ vector. The number of symbols sent from $\boldsymbol{T_X}$ is ($\boldsymbol{M_t} \times 1$), and the received signal at $\boldsymbol{R_X}$ is $\boldsymbol{y = Hs + N}$ (where $\boldsymbol{H = M_r \times M_t}$, is the channel matrix). where $\boldsymbol{s}$ is ($\boldsymbol{M_t} \times 1$) vector. The power constraint on P, considered for transmitting the symbols is represented as $\boldsymbol{E[s * s] \leq Q}$. The additive Gaussian noise at the receiver side is

represented as $\boldsymbol{E[NN^*] = \sigma^2 J_{N_r \times N_r}}$. In this paper, it is assumed that the variation of the noise ($\boldsymbol{\sigma^2}$) is 1.

Considering the precoding and beamforming methods, this paper utilizes SVD-based precoding in a closed-loop MIMO system. Processing the signal/data, the channel matrix $\boldsymbol{H}$ is defined as $\boldsymbol{H = W \wedge X^*}$. The elements W and X are unitary matrix represented as $(\boldsymbol{M_r \times M_r})$ and $(\boldsymbol{M_t \times M_t})$ respectively and $\wedge$ represents the diagonal matrix. At each antenna, the signal interference is eliminated by diagonalizing the channel using precoding at the $\boldsymbol{R_X}$ and decoding is done by CSI. The signal received at $\boldsymbol{R_X}$ is represented as in equation (3 - 6):

$$\boldsymbol{r} = \wedge \widetilde{\boldsymbol{d}} + \widetilde{\boldsymbol{N}} \qquad \textbf{(3)}$$

Where $$\widetilde{\boldsymbol{d}} = V_d \qquad \textbf{(4)}$$

$$\tilde{r} = W^*r \qquad \textbf{(5)}$$

and $$\widetilde{N} = W^*N \qquad \textbf{(6)}$$

The transferred signs can be estimated using a zero-forcing (ZF) or MMSE equalizer. The MIMO loop devices use machine funds to send guide waves for CSI assessment from the point of origin to the recipient and return the CSI. When impulse response errors are entered on the scheme, the process efficiency is also taken into account for reducing reviews by depicting every CSI request in a $\boldsymbol{v}$-bit transparent shape while bringing it home to the receiver. Also, one of the major constraints followed in this proposed approach is investigating the SINR, as the minimum SINR ($SINR < minSINR$) in each transmission.

3.2.3 Channel Autoencoders

Current physical layer training results have demonstrated for single input single output channel [28] that instant encoders [29] can easily suit the efficiency of near-optimum tuning of baselines and coding systems using an autoencoder to know the scheme collectively and it was also shown that this strategy works very well in the air [30]. The concept of the autoencoder of a channel [18, 21] is deeply unmonitored, with a rebuilding-based loss mechanism, so that the coding, decoding and signal display over a certain disabled station can be collectively optimized. Figure-4 shows an illustration of the fundamental signal Single Input Single Output (SISO) autoencoder scheme [34] [35].

This strategy is attractive because it provides tuning and forward error corrections alternative that today stands against current stream deficiency models and provides the finest concepts for tiny code word dimensions and a way of learning alternatives over channel deficiencies that are not renowned for optimizing the alternative. In many instances it can be a less complex computer than current techniques for the encoder and decoder module, resulting in future energy gains when such devices are deployed effectively.

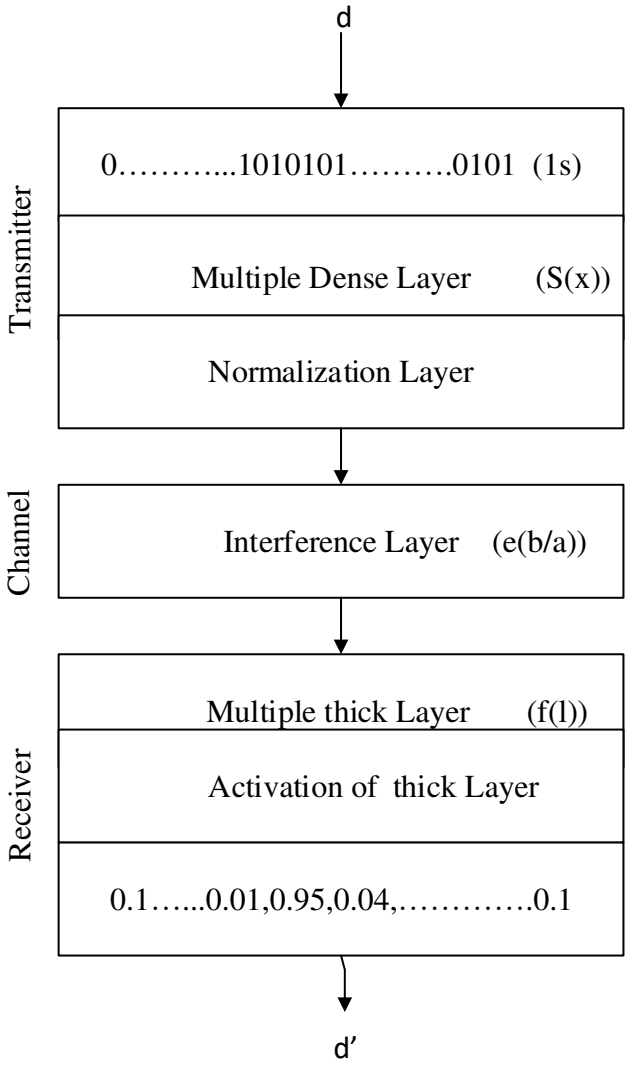

Figure. 4.Single Input Single Output in data encoder

3.2.4 Technical Methodology

Within the autoencoder loop of SISO, $\boldsymbol{k}$-bits will be divided into $\boldsymbol{n}$ linear samples to be sent through some streams such as a disappearing Rayleigh wireless stream. Whenever a decoder receives loud variants of these specimens, the best way is to re-enact the initial data is to calculate e_k. In this paper, we recognize the situation of MIMO where $\boldsymbol{k}$-bits are

represented in $\boldsymbol{m_t}$ parallel specimen flows. The flows are then mixed by a multi-antenna loop and come to a receiver for generating $\boldsymbol{m_r}$ flows, which also have an n-time sample duration and are deciphered for each to generate an evaluation. So, there are distinctive $\boldsymbol{m_r}$ to $\boldsymbol{m_t}$ pair-specific transmissions, each with a certain wireless deficiency.

It is standard in wireless devices, when a MIMO transmission can be recorded continuously in a moment with neighboring samples using various temporal methods, to improve a variable number of transmitting and recipient antennas and signs such as the Alamouti cipher. The transmissions $\boldsymbol{m \times n}$, the received flows $\boldsymbol{m_r}$ and the number of samples $\boldsymbol{n}$ of the data are translated by adjusting the number of segments $\boldsymbol{k}$, so this system can be easily tailored to various data values. The space-time frame encoding, which is optimized for elevated frequency, spatial modulation schemes as well as the enhancement of the variety in reduced frequency can be easily achieved by selects how many parts are stored in a specific space frame.

We introduce the open-loop autoencoder for MIMO channel scheme in Figure (5) to implement and improve a MIMO auto-encoder. This scheme uses multilayer $\boldsymbol{NNs}$ to provide data bits and secret codes encoding for data specimens to be transferred, as well as retrieved data to input parts or coded words from digital specimens. With the absence of any information about CSI, this is an easy way to study encoding, this method is used to get the $\boldsymbol{2 \times 1}$ stream alternative straight likened to Alamouti in section-4, all of which use the normalizing of sequence between layers and $\boldsymbol{s}$ is presented via an integrating element. This method is used straight below.

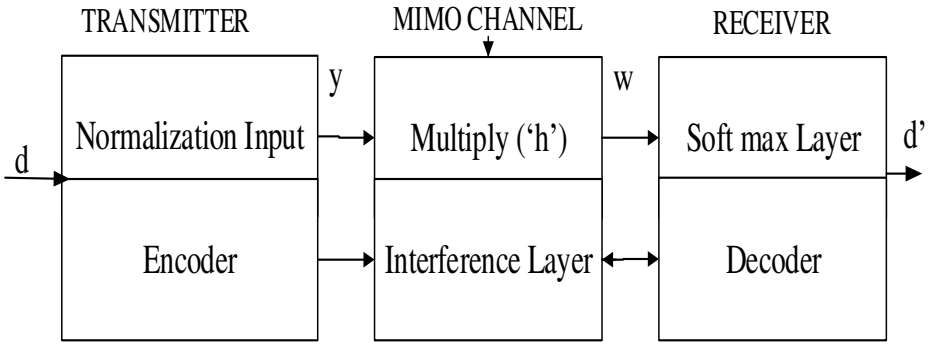

Figure. 5. Autoencoder for MIMO Channel

If there is an ideal CSI of the present disappearing circumstances of the sensor across each tower, then the expansion to this system, as illustrated in Figure (6), is considered which combines $\boldsymbol{s}$ with $\boldsymbol{H}$ before recording for a channel. This easy move is enough, as discussed in section-4, to know a significantly enhanced sustainable output with the present basic systems like **ZF**.

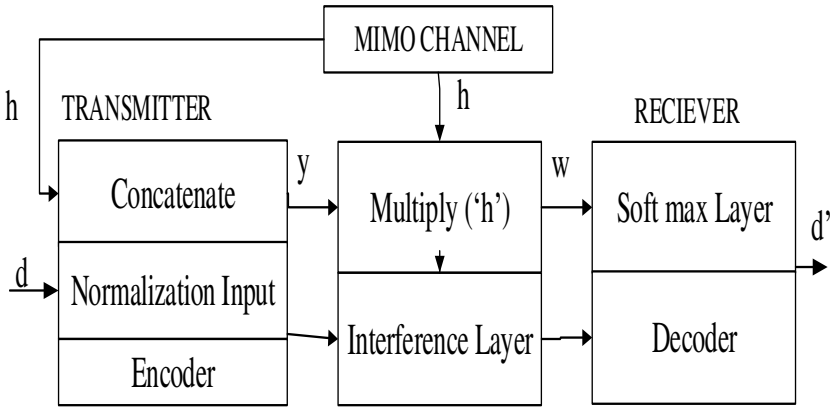

Figure. 6. MIMO Channel with Perfect CSI on data encoder

We are also looking at a CSI situation with measured numbers, representing real-life h understanding, as a separate $\boldsymbol{h_f}$ f-bit matrix. This is essential in actual environment applications, as the capacity to communicate CSI to portable phones most compactly is crucial. Figure. 7 shows MIMO Channel without CSI, that a classified issue on f-bit and $\boldsymbol{2^v}$ is introduced on $\boldsymbol{h_f}$ before reordering and encoding with d to reflect discrete stream conditions.

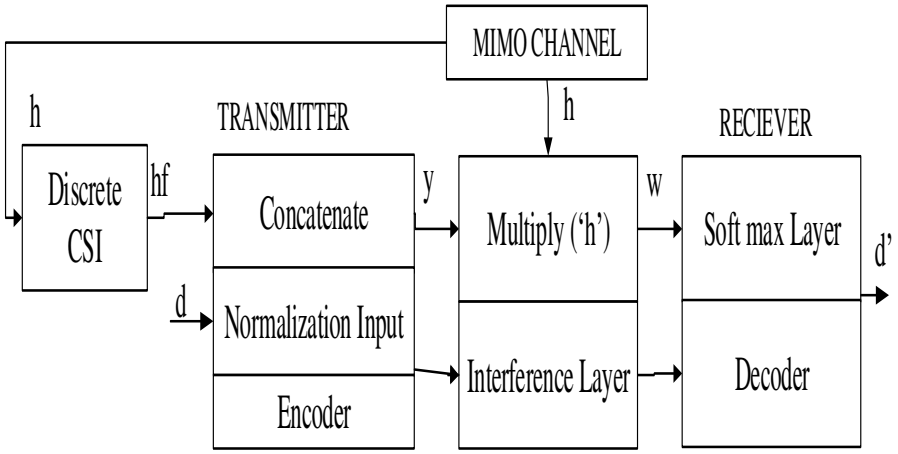

Figure. 7. MIMO Channel without CSI on f-Bit Discrete data encoder

Lastly, the $\boldsymbol{f-bit}$ CSI situation obtained above is taken into consideration. In this instance, a scheme can calculate the recipient's channel $\widehat{\boldsymbol{h}}$, produce a calculation of $\widehat{\boldsymbol{h}}_f$ and communicate this detail for use as programming to the transmitted one. This procedure is streamlined for the symmetrical circuit where $\boldsymbol{h_v}$ can be presumed to be equivalent to 4 in both ways. Figure. 8 shows a completely closed-loop system, which can discover a simple binary CSI feedback technique, encoding, and decoding data via the MIMO disappearing channel. The trained network mapping into a compact CSI type of $\boldsymbol{h_v}$ can, however, learn as shown in Figure. 7, merely by selling the recipient were an expected signal reaction $\widehat{\boldsymbol{h}}$ is acquired using conventional assessment methods or an $\boldsymbol{NN}$ based regressions.

3.2.5 Optimization Process

In this process, d is denoted as an integer codeword (2^k), the length of each codeword is $\boldsymbol{k-bit}$, transmitted in the system. One of the desired codewords is represented as 1, consider as a hot-input and its length is 2^k. The final layer of CNN, i.e, the SoftMax layer classifies each codeword by approximating the probability values of each codeword. A generalized cross-entropy-lose method (y_{EL}) can be used for optimization employing gradient descent to pick network metrics in such ranking assignments. y_{EL} is provided in this situation as:

$$y_{EL}(u,\hat{u}) = \frac{-1}{|u|}\sum_{k=0}^{|u|-1}(u_k \log(r_k)) + (1-u_k)\log(1-r_k)) \qquad (7)$$

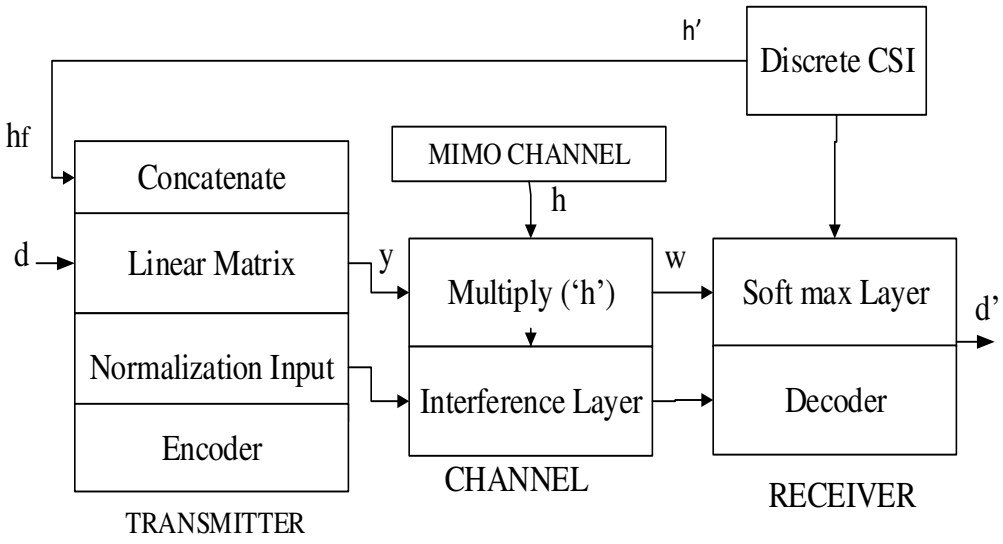

Figure. 8. MIMO with t-Bit CSI for Deployment Scheme

Weight changes depending on the failure gradient are calculated using a type of probabilistic gradient regression [22]. In this example, we calculate a forward transcript:

$$\hat{u} = f(u, \theta) \tag{8}$$

and backward pass

$$\frac{\partial y}{\partial \theta} = \frac{\partial y_{EL}(u, f(u,\theta))}{\partial \theta} \tag{9}$$

also,

$$\delta w = -\eta \frac{\partial y}{\partial \theta} \tag{10}$$

reflects the rate of learning. The layer weight of the network is given as $\boldsymbol{\theta}$. Hence, in this situation, a weight check is a result of the transcript of weight.

4 Deep Convolution Neural Network with Hybrid Infinity (H_∞ - dCNN)

4.1 H-infinity (H_∞) Algorithm:

The H-infinity (H_∞) is proposed to discover the robustness and QoS in the wireless communication networks and it analyze the precoding matrices C. Hence, the precoding observed the fault in the proportion of the i^{th} cell and calculates the interference or noise level found in the entire cell within in the clustered bound. Thus, the H_∞ works for the enormous data information, which transfers through the dCNN and the algorithms communicated initially as follows:

$$\sup_{\tilde{E}_{si}\hat{C}_i H_{i+} w_i} \frac{\|\tilde{E}_{ii}\hat{C}_i H_i\|_X^2}{\|\sum_{s\neq i}^{T} \tilde{E}_{si}\hat{C}_i H_{i+} w_i\|^2} < P \quad (11)$$

Where $\hat{C}_i$ is the estimation work of $C_i$and (10) is equal to,

$$\mathrm{K} = \left\|\sum_{s\neq i}^{T} \tilde{E}_{si}\hat{C}_i H_{i+} w_i\right\| - P^{-1}\left\|\tilde{E}_{ii}\hat{C}_i H_i\right\|_X^2 > 0 \quad (12)$$

The Krein space is used to yield the results (11) is gained into an indefinite quadratic for $\left(\begin{bmatrix} A_i \\ E_{ii}\hat{C}_i H_i \end{bmatrix} - \begin{bmatrix} \tilde{E}_{ii}\hat{C}_i \\ I_N \end{bmatrix} H_i\right)^E \begin{bmatrix} M_N & M \\ M & -P^{-1}X \end{bmatrix} \times \left(\begin{bmatrix} A_i \\ \tilde{E}_{ii}\hat{C}_i H_i \end{bmatrix} - \begin{bmatrix} \tilde{E}_{ii}\hat{C}_i \\ O_K \end{bmatrix} H_i\right) > 0$ (13)

The system of Krein Space alternatively is given by

$$\begin{bmatrix} V_i \\ H'_i \end{bmatrix} = \begin{bmatrix} \widetilde{E}'_{ii} \\ O_N \end{bmatrix} H_i + \begin{bmatrix} y'_i \\ \widetilde{H}_i \end{bmatrix} \quad (14)$$

Where $\mathrm{H'_i} = \widetilde{\mathrm{E}}_{\mathrm{ii}}\hat{\mathrm{C}}_{\mathrm{i}}\mathrm{H},\ \widetilde{\mathrm{H}}_{\mathrm{ii}} = \widetilde{\mathrm{E}}_{\mathrm{ii}}\hat{\mathrm{C}}_{\mathrm{i}},\ \widetilde{\mathrm{H}}_{\mathrm{i}} = \mathrm{H'_i}\mathrm{H}_{\mathrm{i}}$,

$w'_i = \sum_{s\neq i}^{T} \tilde{E}_{si} H_i H_{i+} w_i$. $\tilde{E}_{ii}^{-1}$ is multiplied on both sides, the upper part of (17), it can be rewritten as

$$\begin{bmatrix} \varphi_i \\ H'_i \end{bmatrix} = \begin{bmatrix} M_N \\ M_N \end{bmatrix} H_i + \begin{bmatrix} \tilde{E}_{ii}^{-1} w'_i \\ \widetilde{H}_i \end{bmatrix} \quad (15)$$

Where, $\varphi_i = \widetilde{E}'^{-1}_{ii} V_j$ and the covariance of Θ_i is $Q_{\theta_i} < c_i, c_i >$, whereas, $c_i = [\Theta_i \quad H'_i]^R$ and is given by [11]

$$M_{\theta_i} = \begin{bmatrix} M_N + \gamma_i^{-1} & M_N \\ M_N & M - pX \end{bmatrix} \quad (16)$$

where. $\gamma_j = \widetilde{E}'^{-1}_{ii}\widetilde{E}'_{ii}$

$$T_{\theta_i} = J_i L J_i \quad (17)$$

Where J=diag $\{M_N, -M_N\}, J_j$ *is a* $2N \times 2N$ invertible matrix. The minimum L can be defined as

$$L_{min} = \left\|\check{c}_{\varphi_i}\right\|^2 - \left\|\check{c}_{H'_i}\right\|^2 \quad (18)$$

Equation [18] gives the least values which encompass "L" in the equation [16] and [17]. The existing value at the least that T_{θ_j} has a J-spectral factorization, which could be attained by a closed-form canonical solution

Presumptuous $\sum_j = [\check{c}_{\varphi_i} \quad \check{c}_{E'_i}]^R = J_i^{-1}\mathrm{d}_i$, and

$$J_i = \begin{bmatrix} J_{11} & J_{12} \\ J_{21} & J_{22} \end{bmatrix} \tag{19}$$

Where, $J_{11}, J_{12}, J_{21}, J_{22}$ are the $k \times N$matrices, correspondingly, we introduce a $k \times 1$vector , ψ satisfying $\|\psi\|_\infty$=max($|\psi_1|, |\psi_2|, \ldots, |\psi_k|$) < 1 to guarantee L_{min}>0 and we get

$$\check{c}_{G'_i} = \psi \check{c}_{\varphi_i} \tag{20}$$

Substituting (23) and Θ_i into $\Sigma_i, we\ obtain$

$$\begin{bmatrix} \check{c}_{\emptyset_i} \\ \psi \check{c}_{\varphi_i} \end{bmatrix} = J_i^{-1} \begin{bmatrix} \emptyset_i \\ H'_i \end{bmatrix} \tag{21}$$

And

$$\begin{bmatrix} \emptyset_i \\ H'_i \end{bmatrix} = \begin{bmatrix} J_{11}\check{c}_{\emptyset_i} & J_{12}\psi\check{c}_{\emptyset_i} \\ J_{21}\check{c}_{\emptyset_i} & J_{22}\psi\check{c}_{\emptyset_i} \end{bmatrix} \tag{22}$$

Now, we find that the design of the H-inf precoding primarily depends on J- spectral factorization of T_{θ_i} .

$$H'_i = J_2\, J_1^{-1} \widetilde{E'}_{ii}^{+} Z_i \tag{23}$$

where $J_1 = J_{11} + J_{12}$.

4.2 H-infinity Precoding closed method:

In this closed form of H-infinity is considered to obtain from equation (19) and (20) as written in equation (24)

$$Q_{\theta_i} = \begin{bmatrix} \widehat{J}_{1,1} & \widehat{J}_{1,2} \\ \widehat{J}_{2,1} & \widehat{J}_{2,2} \end{bmatrix} \begin{bmatrix} M_K & M \\ M & -M_N \end{bmatrix} \begin{bmatrix} \widehat{J}_{1,1} & \widehat{J}_{1,2} \\ \widehat{J}_{2,1} & \widehat{J}_{2,2} \end{bmatrix}^F \tag{24}$$

Where $\widehat{J}_{1,1}$, $\widehat{J}_{1,2}$, $\widehat{J}_{2,1}$, $\widehat{J}_{2,2}$ is a group of conforming answers $\widehat{J}_{1,1}$, $\widehat{J}_{1,2}$, $\widehat{J}_{2,1}$, $\widehat{J}_{2,2}$ by Resolving.

Hence, the H-infinity algorithms are utilized the dCNN for transmitting the infinity number sample data to the receiver through the MIMO channel. The main factor for optimizing the entire system is, the accuracy of the MIMO stream impacts in the network transition function $\hat{s} = f(s, \theta)$. For this purpose, we present several fresh levels simulating actual universe impairments and layout restrictions for each forward or reverse the move.

Following encryption to m_t complicated evaluated transmitter packets, a transmitter block-code matrix of the form (sample-length, m_t 2, n), which contains true and imagery characteristics are created for transmitting. It can also be used with multiple custom levels to mimic MIMO transmission to model the following domain. The deep learning algorithms are structured by using the algorithms is as follows

The input transmission data (d) is transmitted to insisted by using the encoder as y

enco : encodes the information: $d \longmapsto y$

rnd : Random number of transmitter and receiver $n_r \times n_t$*, channel response h*

mux : Multiply the complex matrix of y with h

norm : average signal power is quite nomoralized

gn : white gaussian noise wgn $(0, \sigma)$

deco: decodes the information $r \longmapsto d'$

Hence the open-loop MIMO system is implemented with the infinity of information by the deep learning, it enhances the encoder to perform the complete network 'f ' is given in equation (25)

$$f(d,\theta) = dec(gn(norm(mul(enco(d), rnd())), \sigma)) \quad (25)$$

and the decoding process of the MIMO closed-loop (26) is represented as:

$$f(d,\theta) = (\lambda h, deco(awg\big(norm\big(mul(enco(d,h),h)\big),\sigma\big)))(rnd()) \quad (26)$$

This version allows for easy calculation of forward and reverses gradient runs for f(d, θ). The awg feature becomes the identification feature in the reverse pass (the feature is only used for the forward pass). The noise variation σ can be readjusted readily during practice or during tests to simulate variable concentrations of SNR, whereas the normalization unit imposes a continuous median authority.

4. Results and Discussions

In this chapter, we practice the above-defined auto-encoder-based trained routing system, assess the efficiency of the bit error rate (BER) over the separate SNRs, and contrast the output to commonly used cable baselines. For both spectral diversity and multipathing, MATLAB is used to simulate the standard MIMO schemes. For DL automatic execution, a powerful GPU backend, Keras with Tensorflow is used. In the simulation-based experiment, the performance of the proposed deep learning-based MIMO with proposed antenna design

strategies is verified using two different configurations such as 2×1 Alamouti STBC used to provide variations in the temporal communication range for increasing the performance, and 2×2 MIMO system involving spatial multiplexing. During the transmission, the QPSK modulation is used for modulating the input data over the Rayleigh fading channel are used in the simulation. To do designing triband monopolies antenna the antenna toolbox is installed in MATLAB software and the results are verified. The QPSK modulation is applied with Alamouti coding on each signal to noise ratio with/without coupling. The system operating frequency is 2.4GHz and it is changed during execution. The SNR range is also changed for verifying the performance. At each iteration, the SNR value is changed with and without antenna coupling for performance evaluation. Based on the iteration, the learning capacity of the deep CNN model is increased. The learning capacity of CNN determines the classification accuracy of the network configurations.

4.1 Spatial Diversity

Alamouti coding organizations symbolize two timeframes sequentially. In the first space, it receives two distinct signs from each receiver. Usually, the bits are demodulated by an MMSE recipient. In auto coding, s can describe the same number of bits (4), that describe two-bit symbols, the same density as in our simulation as defined above. Likewise, the autoencoder carries these fragments out into two later complicated true timepieces that are equal to the transmitted density of the Alamouti. The transmitter does not have a CSI (e.g. open-loop MIMO) accessible.

Initially, the performance of the proposed learning method is verified by investigating the BER. Figure-10 shows the BER curve for the encoding method without CSI and Alamouti coding (2 x 1). The baseline with perfect CSI obtained lesser BER than the autoencoding without CSI. The proposed autoencoder obtained above 20dB of SNR for $0.5e^{-5}$ BER. The average BER value is calculated for all the antennas is given here. The autoencoder provided a promising output comparing with the baseline method. One of the major advantages is, this method applies the mapping and de-mapping process for correcting the inherent error. For both Alamouti STBC and the auto-encoder systems, Figure. 10 demonstrates the SNR vs. BER outcomes. From the results, it is clear that the Alamouti STBC has mildly enhanced efficiency at small SNR and enhanced self-encoder efficiency above approximately 15dB. We are satisfied that these outcomes can be produced without important hyper-parameter adjustments or lengthy learnings and that these findings

eventually have considerable capacity for enhancement. From Figure-10, it can be identified that the BER in terms of SNR for 2x1 and 2x2 Alamouti-STBC method including autoencoder is better and the performance is improved 15dB from the autoencoder. Improvement in the performance due to tuning the hyper-parameter and training the model with a higher number of iterations.

Figure.11 shows countless discrete drawings in the constellation points of the signal matrix H. In this situation, the system seems to have learned in this situation to attain its median power transmission via irregular power generation between the two antennas. From the channel matrix **H**, based on the massive random points draw the constellation points. The proposed deep learning method learn the entire dynamic behavior of the network and obtained the average Tx power. It can be done over the uneven power distribution among two antennas and get the super-position coding method. The same constellation is shown in Figure.12. Similar constellation for a constant H, for the superposition in Tx, between 1 and 2 antennas available in the Rx side. This superposition style constellation is merely similar to the SISO interference discussed in [23, 24]. Figure-11 shows the random channel points and Figure-12 shows the diagonal channel points. The main difference is the superposition of the constellation.

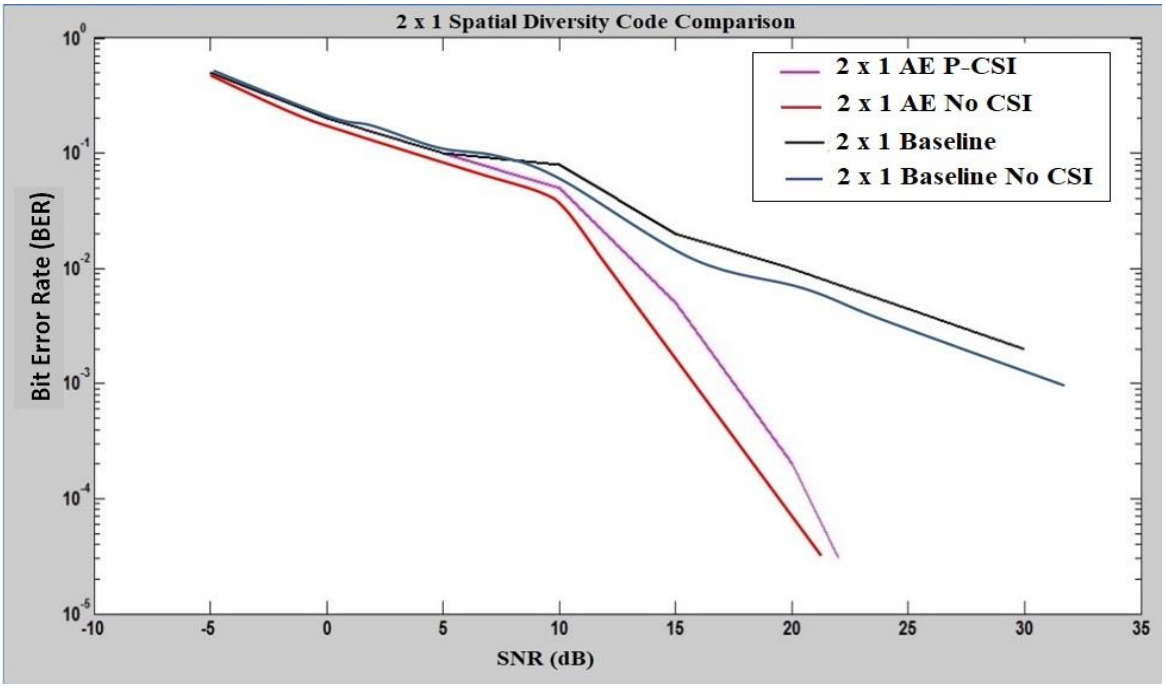

Figure. 10. Performance of error rate in Diversity Scheme

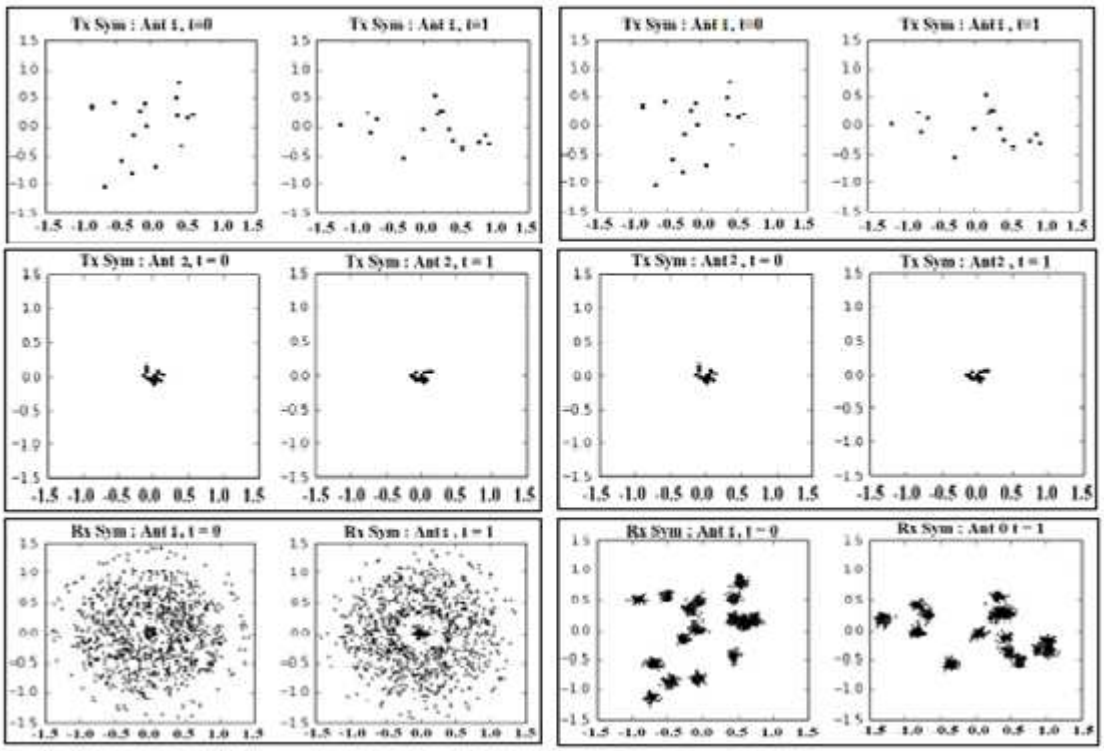

Figure.11. 2x1- Random Channels **Figure.12.** 2x1- Diagonal Channel.

4.2 Spatial Multiplexing

We examined the efficiency of two distinct settings; if the CSI is ideal and CSI is quantified at the space multiplexing receiver. 1) Ideal Channel Data on a Sender: A 2x2 MIMO loop with a one-time slot, using both a standard transmission scheme and an auto-encoder strategy, is simulated. The signal assessment is presumed to be ideal and input is absent when the CSI is returned to the receiver. Rayleigh distortion is used as the stream method and the same energy is used for the basis and auto-encoder processes in each satellite.

To diagonalize the stream and minimize distortion in the basic technique, the transmitter utilizes CSI for the SVD-based precoding. The simulation consists of 100 subframes each with 1000 signs. The consistency time of the stream is presumed to be equivalent to the entire length of a subframe. Therefore for 1000 characters, the same stream estimate is used and for each subframe, the stream estimate is repeated. The median outcomes of the BER are calculated by the antenna for all signs and subframes and the BER outcomes per antenna are measured again to achieve ultimate BER output curves. The Auto Encoder generator also integrates ideal CSI data directly into the recording method. As a consequence, during practice, the signal impact on the code transferred is efficiently understood and the data for the receiving person is better preserved.

Secondly, the transmitter is considered with deep learning involved autoencoder integrated with perfect CSI. According to this the result of the channel available at the Rx side influences the transmitted symbols, where has been learned by the deep learner at the training phase. From the learned information, it provides the best prior knowledge for the receiver. We provide the BER efficiency curve of the deep learning involved encoding method in Figure.13 associated with the baseline with CSI situation. The complete median BER outcomes are given for both detectors. Here, we get highly successful outcomes relative to the standard technique, possibly from an intrinsic error checking system incorporated in tracing and deduction, as we have seen in [18]. This is a strategy that can be highly effective. An exciting construct is revealed by checking the transmission and the receipt of constellations for the 2x2 system. Figure.14 and Figure.15 illustrate constellations for the **H** border as well as for the **H** all-one matrix. In Figure.14 we can demonstrate constellations on a set of separate signal drawings. Intriguingly, we seem to have a received waveform with almost continuous frequency stage modulation for an H material with approximately standardized energy for each signal while the transmitter constellations claim to render schemes with $\mathbf{2^k = 16}$ pieces, forming a pseudo-standard system of the 16QAM sort.

4.3 Quantization Process

Our next stage is for the simulated response mistake to represent the practical difficulties of the application. Because CSI's reviews for closed-loop plans (for example, from a cell/mobile to ground-station) involves overload protocols in actual system applications, we will recognize the situation in which CSI is restricted to the compressed, permanent and valuable data transmitted into a narrow v-bit domain. For the basis MIMO scheme, we've used Lloyd algorithms for quantifications. The quantizer was usually assigned random digits. Both the generator and recipient are aware of the quantization scores beforehand so that the recipient gives v-bit indices of the stream data to a generator.

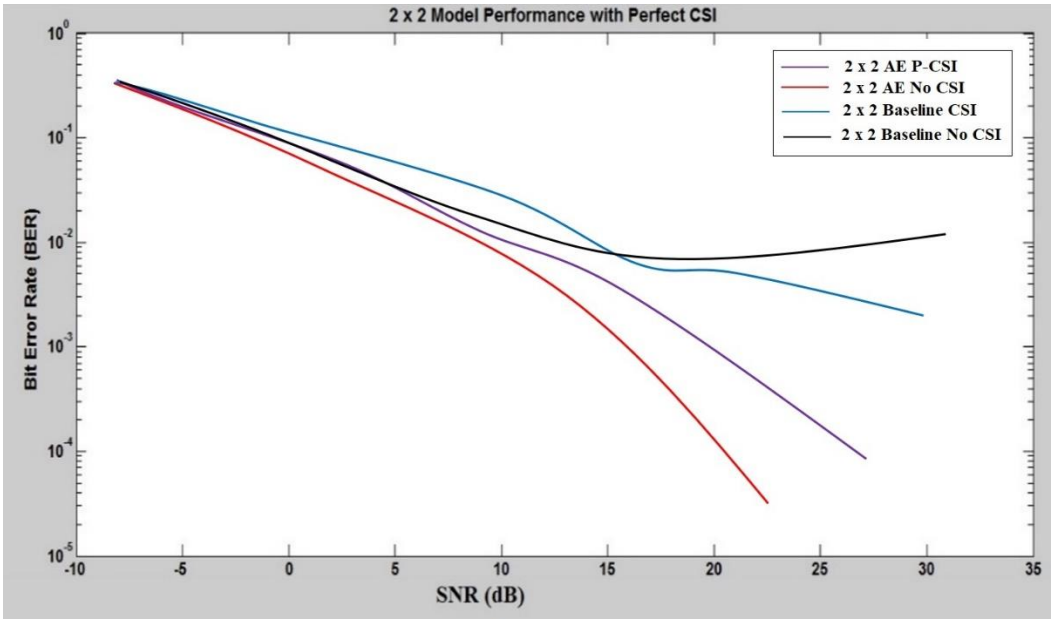

Figure.13. Error Rate Performance of perfect CSI in 2x2 Scheme

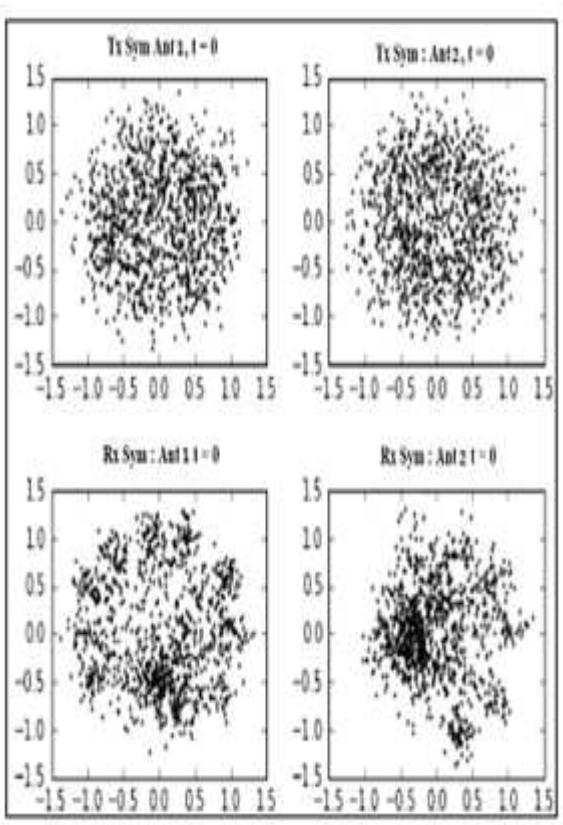

Figure.14. 2x2 - Random Channels.

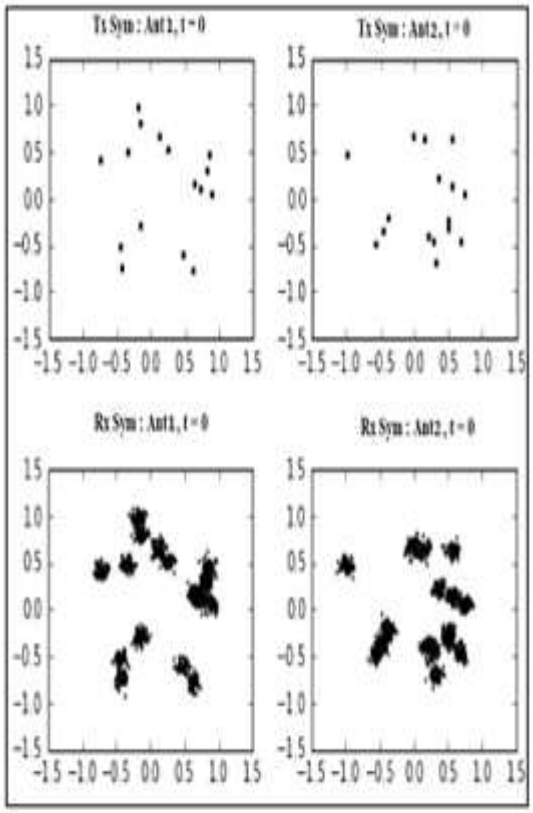

Figure.15. 2x2 - Diagonal Channel.

The structure efficiency closely resembles the perfect 8-bit quantized CSI case, but the number of quantizing bits decreases as shown in Figure 16.

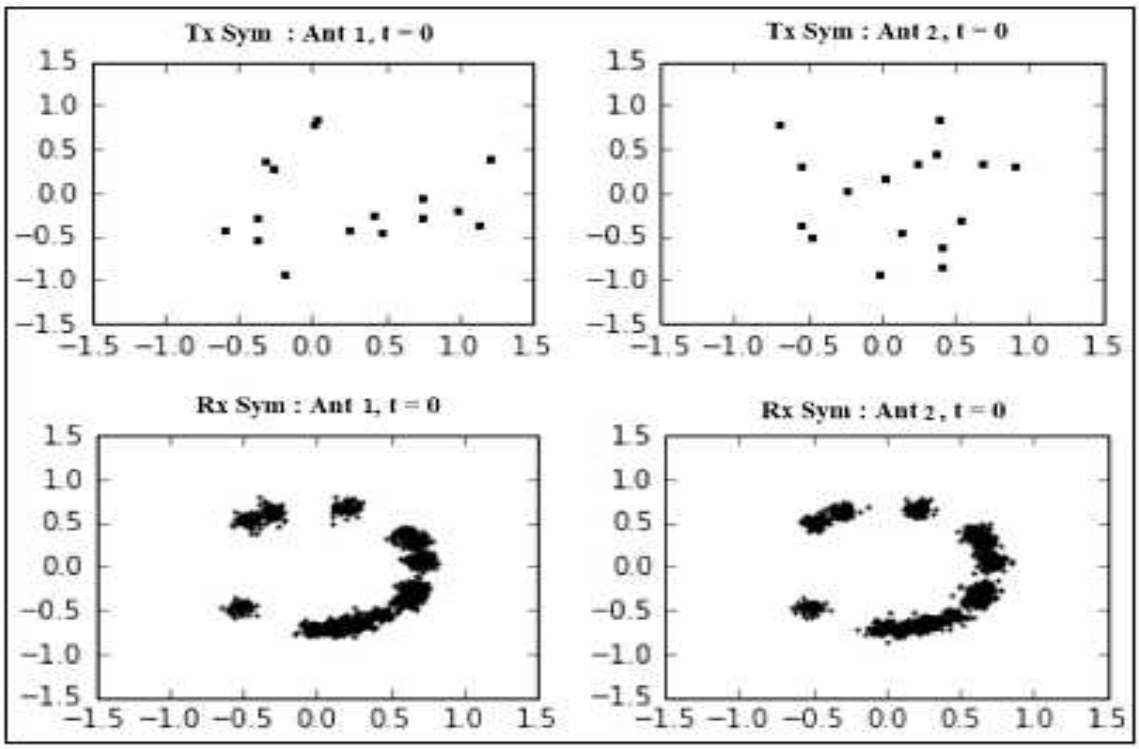

Figure.16. All Single Channel with 2x2 Scheme

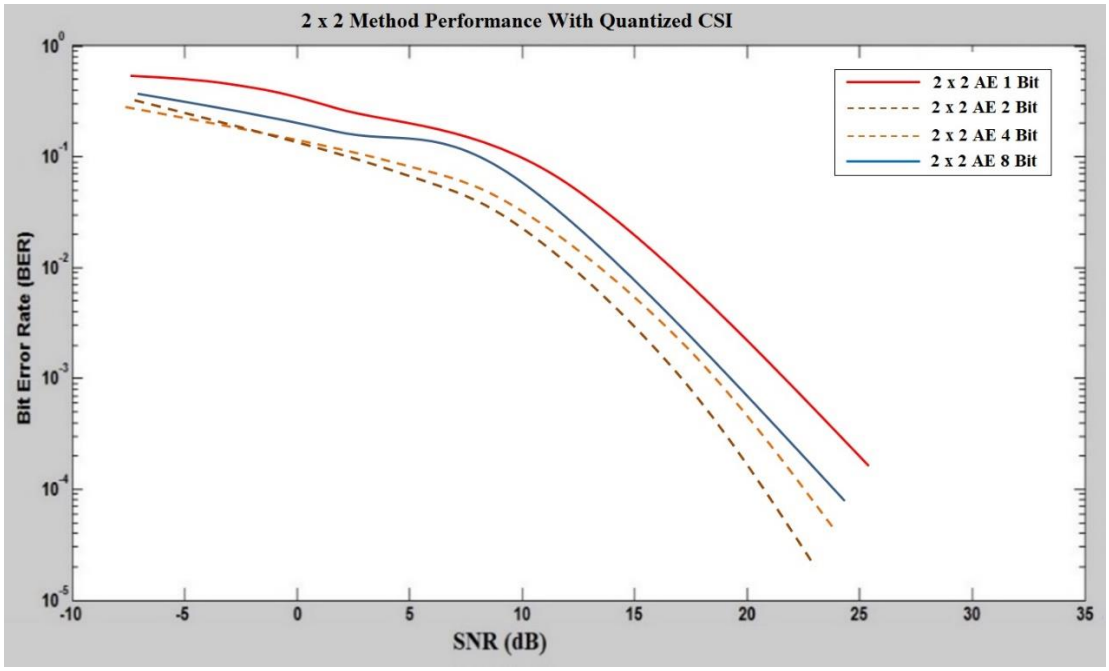

Figure.17. Error Rate Performance of Baseline 2x2 Scheme (Quantized CSI).

In the autoencoder scenario, we can simply see an increase in performance in some of the quantized CSI cases (2, 4- and 8-bit CSI) compared with the optimal casing of the CSI when examining the BER curve outcomes for the base-line technique of Figure 17, as we comprise CSI with fewer bits. Quantifying the CSI in 2^v separate models enables the trained

scheme to progress to an encoder setup for each stream type more readily. This is probably a far more simple goal manual rather than trying to adjust the complete complicated routing from a true H to some respective true encoder types and it appears to offer a better way to enhance BER across a broad variety of SNR concentrations while also making a success of aerial delivery and using in potential wireless norms alongside co-operation.

Best Approach: We demonstrate the finest auto coder strategy among those assessed in Figure 20 to summarize our results for the 2x2 transmitting system and comparing it to the basic results. The efficiency over the full operating spectrum improved significantly with BER output below 0.6e to 5 below and SNR below 20dB. In our opinion, this is a strong outcome that carries huge promises for use in potential mobile and local area network applications, offering an incredibly compact manner to achieve a solid MIMO encoding system that offers a high level of error detection and a much better efficiency relative to present standards.

The findings in our proposed system evaluated and modelled where S-parameters are drawn up and a healthy consensus is reached between them. This proposed deep learning-based MIMO transmitter works across frequencies ranges of (2.4GHZ, GHz, 3,4-3.7GHZ, 5,15-5.35, and 5.725-5.825 and 3.1-10.6GHZ, respectively less than 21, 33 and 42dB mutually interconnected. Most WiMAX and wireless channels are covered by the working frequency spectrum. Measured radiation models are provided at 2.4, 3.5, and 5.8GHz frequencies with one port. Such stabilization in the primary beam design generated excellent radiation features in the suggested transmitter which were excellent collimation of beams, smooth primary beams, and small lateral bends. Differences in the present allocation of both frequencies can result in the reduced dissipations of the decoupling and matching network at the greater frequency. By the use of various antennas both at the transmitter and at the receiver, MIMO devices improve the broadcast capability significantly and without increased transmitter energy or device bandwidth.

5. Conclusion

The main objective of this paper is to improve QoS in wireless communication systems. Hence this paper proposed a novel system that has a two-stage system. The first is to employ the multiband antenna for wireless network computing, and the next is to optimize resource allocation and carrier detection as well as other criteria for improving service quality by analyzing the network behavior using Deep Learning Algorithm. The working bandwidth

can be enhanced by adding the network of connections to the antenna terminals, by reducing the original interconnected connection and impedance errors detected. The findings show that the strip-coupled splinter carrying system activated the resonance of the shell of the substrate efficiently. Over the whole, the antenna with the specified acquired excellent radiation characteristics. The prevalent (accessible) bandwidth is especially enhanced. The suggested decoupling technique is compact with the easier dimensions relative to most standard multi-band MIMO antennas because of the double feature of long inverted-L stub and the tiny occupied area of tap-shaped lines. The suggested MIMO transmitter is performing well and can be incorporated with different terminals in wireless and WiMAX bands with a compact design.

Considering the efficiencies of the proposed antenna, it is decided that, for any wireless applications, using a multi-band MIMO antenna can provide better efficiency in terms of impedance, bandwidth from 2.65GHz to 6.8GHz resonant frequencies. It is also concluded that the proposed antenna can be used for any 5G applications. This proposed deep Convolution Neural Network (dCNN) with Hybrid Infinity (H_∞) is implemented using MATLAB software and the results are verified. It is compared with the conventional methods for evaluating the performance of the dCNN, and proved that dCNN outperforms than other existing methods.

Summary

From the overall explanation and obtained experimental results, the efficiency of proposed deep learning is summarised as:

Initially, the input is verified and with noisy constellation points at high SNR (20dB) to deep learning in a 2 x 1 system. It was very interesting while learning the constellations and it is obtained that, for 1-bit CSI, both antenna-0 and antenna-1 transmit two different power based constant modulus encodings by learning the multilevel scheme.

The autoencoder is trained by the proposed deep learning model and obtained the BER over a defined range of SNR values. It is compared with the baselines under various channel conditions (which is widely used). To simulate the proposed learning method MATLAB is used. Initially, a conventional MIMO system experiments in terms of spatial diversity and spatial multiplexing. In deep learning, the TensorFlow and Keras backend are incorporated. In the simulation 2x1 and 2x2 Alamouti STBC model is used for improving the performance in terms of spatial diversity and spatial multiplexing. For the defined K-bit size

K-bit QPSK modulation method is applied for modulating the input over the Rayleigh fading channel model. Also, it is noticed that the deep learning algorithm learned a complex multi-level communication method, irregular 16-QAM on every Tx, where the output signal, for the same power paths, it provides a constant modulus.

This proposed method is considered as the best method because autoencoder outperforms than the baseline. Also, a significant improvement is obtained in terms of BER lesser than $0.6e^{-5}$ and the SNR lesser than 25dB, which is comparatively best than the baseline method.

Declarations:

Funding

Authors did not receive any funding.

Conflicts of interests

Authors do not have any conflicts.

Availability of data and material

Available on request.

Code availability

Not applicable.

Authors' Contributions

C. Priya, D. Kumutha, M. Shilpa, K. Jayanthi and S. Baskaran are authors of the manuscript. They read and approved the manuscript.

References

1. N. Taspinar and M. Yildirim, "A Novel Parallel Artificial Bee Colony Algorithm and Its PAPR Reduction Performance Using SLM Scheme in OFDM and MIMO-OFDM Systems," in IEEE Communications Letters, vol. 19, no. 10, pp. 1830-1833, Oct. 2015.

2. YantaoQiao, Songyu Yu, PengchengSu and Lijun Zhang, "Research on an iterative algorithm of LS channel estimation in MIMO OFDM systems," in IEEE Transactions on Broadcasting, vol. 51, no. 1, pp. 149-153, March 2005.

3. Kumutha, D., & Prabha, N. A. (2006). Effective PAPR Reduction in MIMO-OFDM using combined SFBC-PTS'. ARPN J Eng Appl Sci, 11(21), 12690-12694.

4. Kumutha, D., & Prabha, N. A. (2016). Performance analysis of PAPR reduction in LTE system. Indian Journal of Science and Technology, 9(32), 1-9.

5. Suganya, R., Kumutha, D., & Amutha Prabha. (2016), N. Improvement of BER using Pilot Insertion with SSS Algorithm in Sparse Channel Estimation, International Journal of Research Development and Organization (IJRDO) – 30-June, 2273.

6. Y. LeCun, Y. Bengio, and G. Hinton, “Deep learning,” Nature, vol. 521, no. 7553, pp. 436–444, 2015.

7. J. R Hershey, J. L. Roux, and F. Weninger, “Deep unfolding: Model-based inspiration of novel deep architectures,” arXiv preprint arXiv:1409.2574, 2014.

8. T. J. OShea and j. Hoydis, “An introduction to machine learning communications systems,” arXiv preprint arXiv:1702.00832, 2017.

9. K. Gregor and Y. LeCun, “Learning fast approximations of sparse coding,” in Proceedings of the 27th International Conference on Machine Learning (ICML-10), 2010, pp. 399–406.

10. M. Borgerding and P. Schniter, “Onsager-corrected deep learning for sparse linear inverse problems,” arXiv preprint arXiv:1607.05966, 2016.

11. Manogaran, G., Shakeel, P. M., Fouad, H., Nam, Y., Baskar, S., Chilamkurti, N., & Sundarasekar, R. (2019). Wearable IoT smart-log patch: An edge computing-based Bayesian deep learning network system for multi access physical monitoring system. *Sensors*, *19*(13), 3030.

12. A. Mousavi and R. G. Baraniuk, “Learning to invert: Signal recovery via deep convolutional networks,” arXiv preprint arXiv:1701.03891, 2017.

13. P. Zhu, L. Tang, Y. Wang and X. You, "Time-Domain Compression Based Analog Feedback for MIMO-OFDM Systems," in IEEE Communications Letters, vol. 17, no. 7, pp. 1412-1415, July 2013.

14. Hua Zhang, Y. G. Li, A. Reid and J. Terry, "Optimum training symbol design for MIMO OFDM in correlated fading channels," in IEEE Transactions on Wireless Communications, vol. 5, no. 9, pp. 2343-2347, September 2006.

15. Y. Kang, M. Min and G. Im, "Grouped Channel Quantization and Antenna Combining for Multiuser MIMO OFDM Systems," in IEEE Communications Letters, vol. 18, no. 12, pp. 2217-2220, Dec. 2014.

16. T. Jiang, C. Ni and L. Guan, "A Novel Phase Offset SLM Scheme for PAPR Reduction in Alamouti MIMO-OFDM Systems Without Side Information," in IEEE Signal Processing Letters, vol. 20, no. 4, pp. 383-386, April 2013.

17. S. Biswas, K. Singh, O. Taghizadeh and T. Ratnarajah, "Coexistence of MIMO Radar and FD MIMO Cellular Systems With QoS Considerations," in IEEE Transactions on Wireless Communications, vol. 17, no. 11, pp. 7281-7294, Nov. 2018.

18. G. Xu et al., "Full Dimension MIMO (FD-MIMO): Demonstrating Commercial Feasibility," in IEEE Journal on Selected Areas in Communications, vol. 35, no. 8, pp. 1876-1886, Aug. 2017.

19. Kumutha, D., Arulmozhi, S., Meena, K., Kumar, T. S., Madhumitha, K., & Aswini, K. (2019, March). A Novel Broadband and High-Isolation Dual Polarized Microstrip Antenna for 5G Application. In 2019 International Conference on Vision Towards Emerging Trends in Communication and Networking (ViTECoN) (pp. 1-6). IEEE.

20. Kumar, T. S., & Kumutha, D. (2020). Comparative Analysis of the Fuzzy C-Means and Neuro-Fuzzy Systems for Detecting Retinal Disease. Circuits, Systems, and Signal Processing, 39(2), 698-720.

21. Q. Wang, Z. Wang and L. Dai, "Asymmetrical Hybrid Optical OFDM for Visible Light Communications With Dimming Control," in IEEE Photonics Technology Letters, vol. 27, no. 9, pp. 974-977, 1 May1, 2015.

22. A. Toktas and A. Akdagli: “Wideband MIMO antenna with enhanced isolation for LTE, WiMAX and WLAN 'mobile handsets,” *Electron. Lett.***50** (2014) 723 (DOI: 10.1049/el.2014.0686).

23. Y. Sun, Z. N. Chen, Y. Zhang, H. Chen, and T. S. P. See, “Subwave-length substrate-integrated Fabry-Pérot cavity antennas using artificial magnetic conductor,” *IEEE Trans. Antenn. Propagat.*, vol. 60, pp. 30-35, 2012.

24. T. J. O’Shea and J. Hoydis, “An introduction to deep learning for the physical layer,” CoRR, vol. abs/1702.00832, 2017. [Online]. Available: http://arxiv.org/abs/1702.00832.

25. I. Goodfellow, Y. Bengio, and A. Courville, Deep learning. MIT press, 2016.

26. S. Dorner, S. Cammerer, J. Hoydis, and S. ten Brink, “Deep learning-based communication over the air,” ArXiv preprint arXiv:1707.03384, 2017.

27. T. J. O’Shea, K. Karra, and T. C. Clancy, “Learning to communicate: Channel auto-encoders, domain specific regularizes, and attention,” in 2016 IEEE International Symposium on Signal Processing and Information Technology (ISSPIT), 2016, pp. 223–228. DOI: 10.1109 / ISSPIT.2016.7886039.

28. D. Kingma and J. Ba, “Adam: A method for stochastic optimization,” ArXiv preprint arXiv:1412.6980, 2014.

29. Yang Yang, Yang Li, Kai Li, Shuang Zhao, Rui Chen, Jun Wang, And Song Ci, (2018), “DECCO: Deep-Learning Enabled Coverage and Capacity Optimization for Massive MIMO Systems”, Vol. 6, pp. 23361-23371, DOI:10.1109/ACCESS.2018.2828859.

30. Suganya, R., Kumutha, D., & Amutha Prabha. (2016), N. Improvement of BER using Pilot Insertion with SSS Algorithm in Sparse Channel Estimation, International Journal of Research Development and Organization (IJRDO) – 30-June, 2273.

31. R.Shanthakumar, D.Kumutha, S.Balaji, Dr.N.Amutha Prabha, “OFDM Based Encryption and Decryption Techniques for Wireless Transfer of Sensitive Data”, published a research paper in IJAER, Volume 10, No.30 (2015), - ISSN (Online):0973-4562, ISSN (Print): 22903-22908.

32. T. J. O’Shea and J. Hoydis, “An introduction to deep learning for the physical layer,” CoRR, vol. abs/1702.00832, 2017. [Online]. Available: http://arxiv.org/abs/1702.00832.

33. D.Kumutha, “Reduction of Peak to Average Power Ratio using Block Coding Schemes in MIMO – OFDM System”Thesis-VIT University, http://hdl.handle.net/10603/264932.

Figures

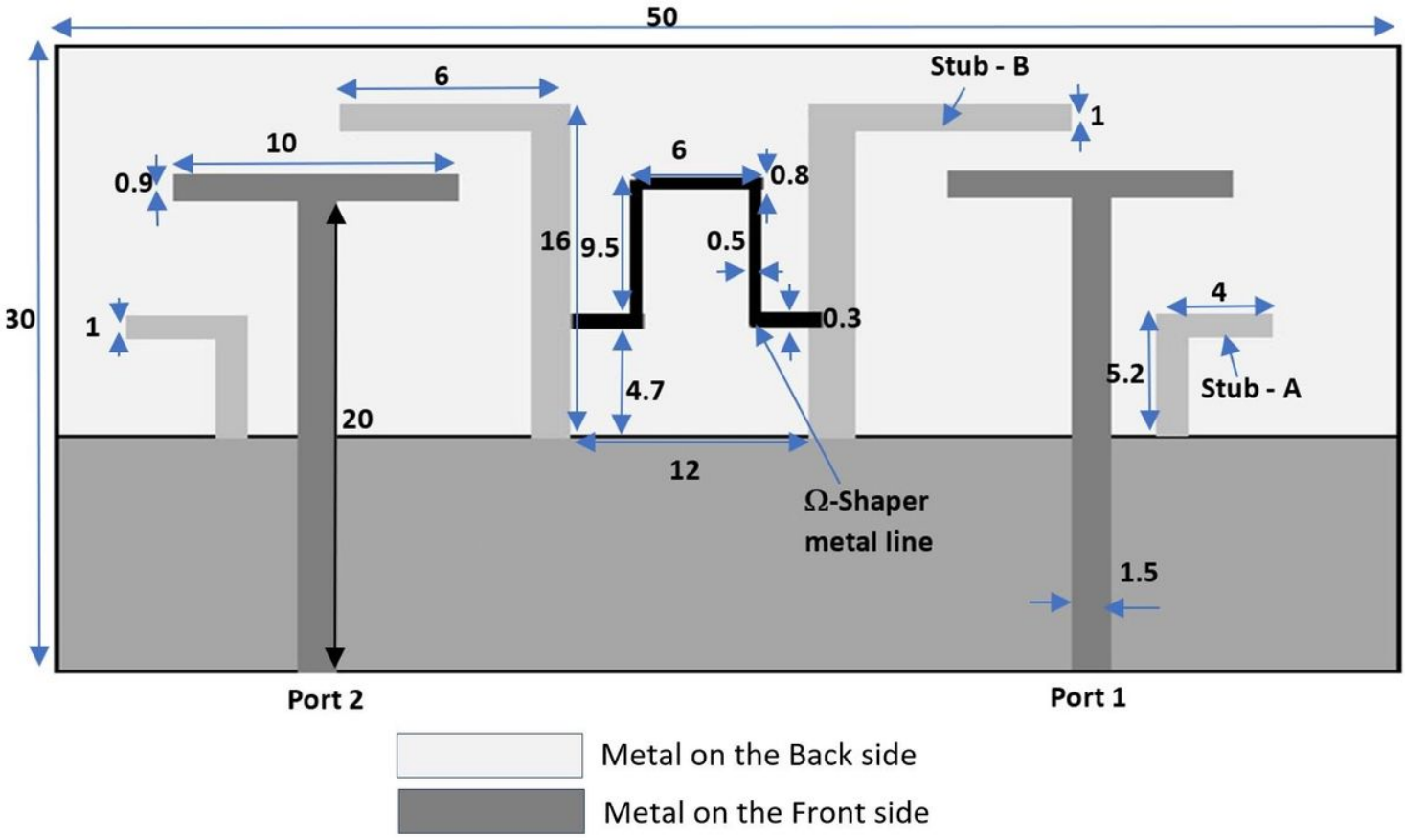

Figure 1

Multiple Antenna System

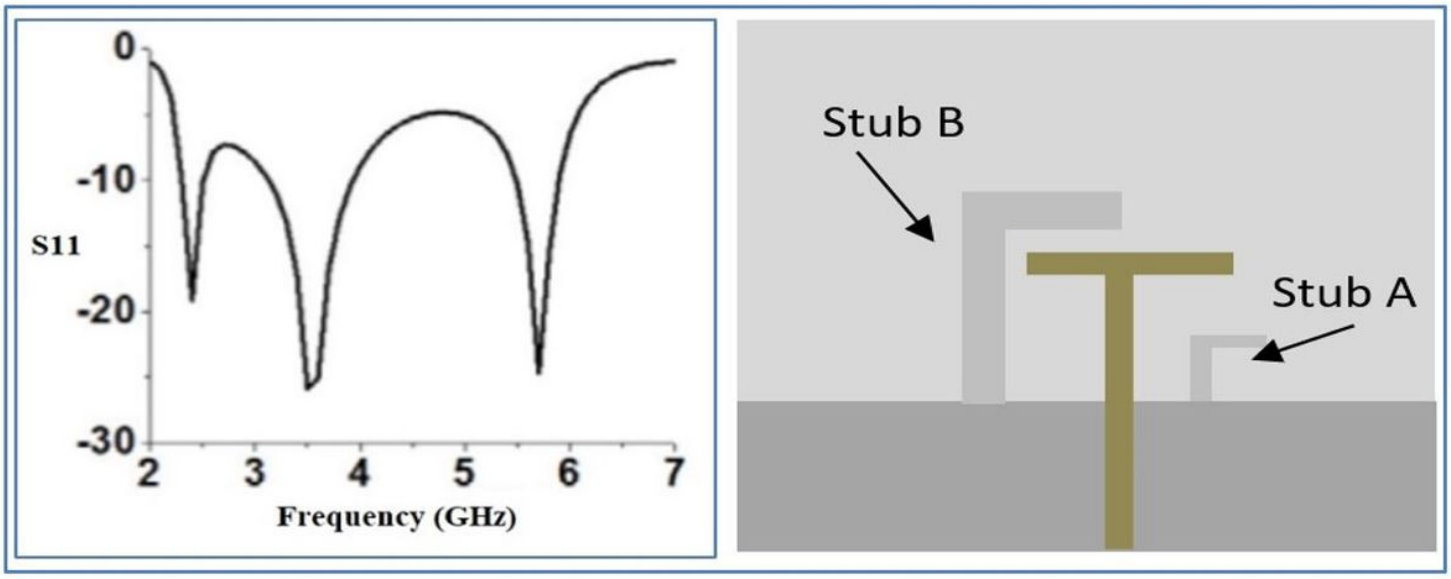

Figure 2

(a). Triband Monopole(S11) (b). Triband Monopole

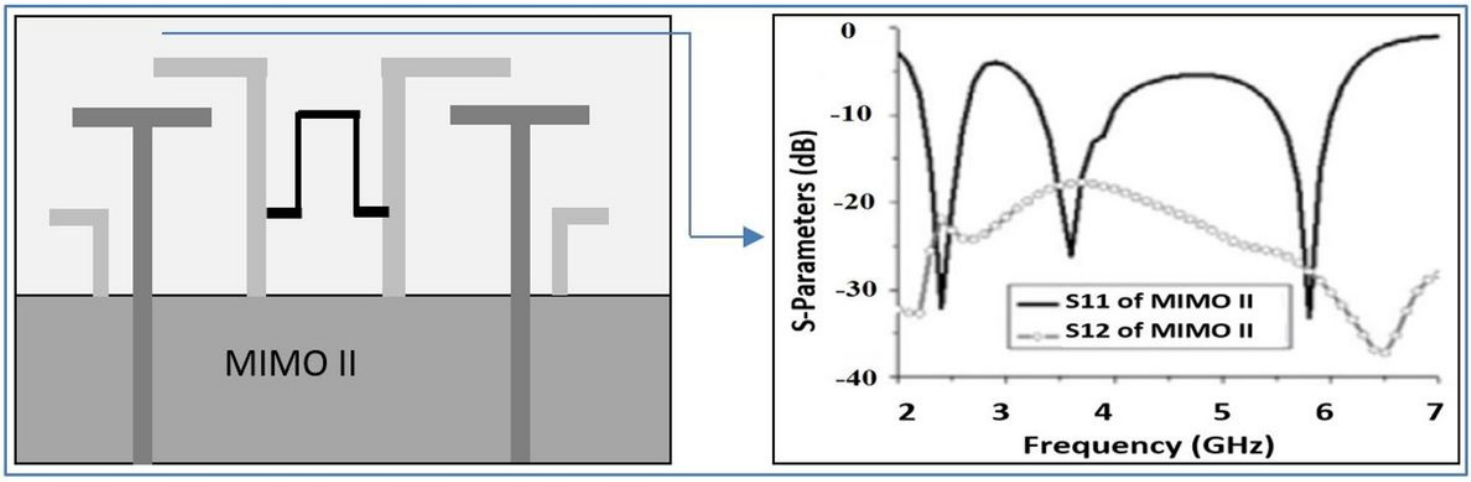

Figure 3

(a) Symbol of MIMO II (b) MIMO II's S-parameters

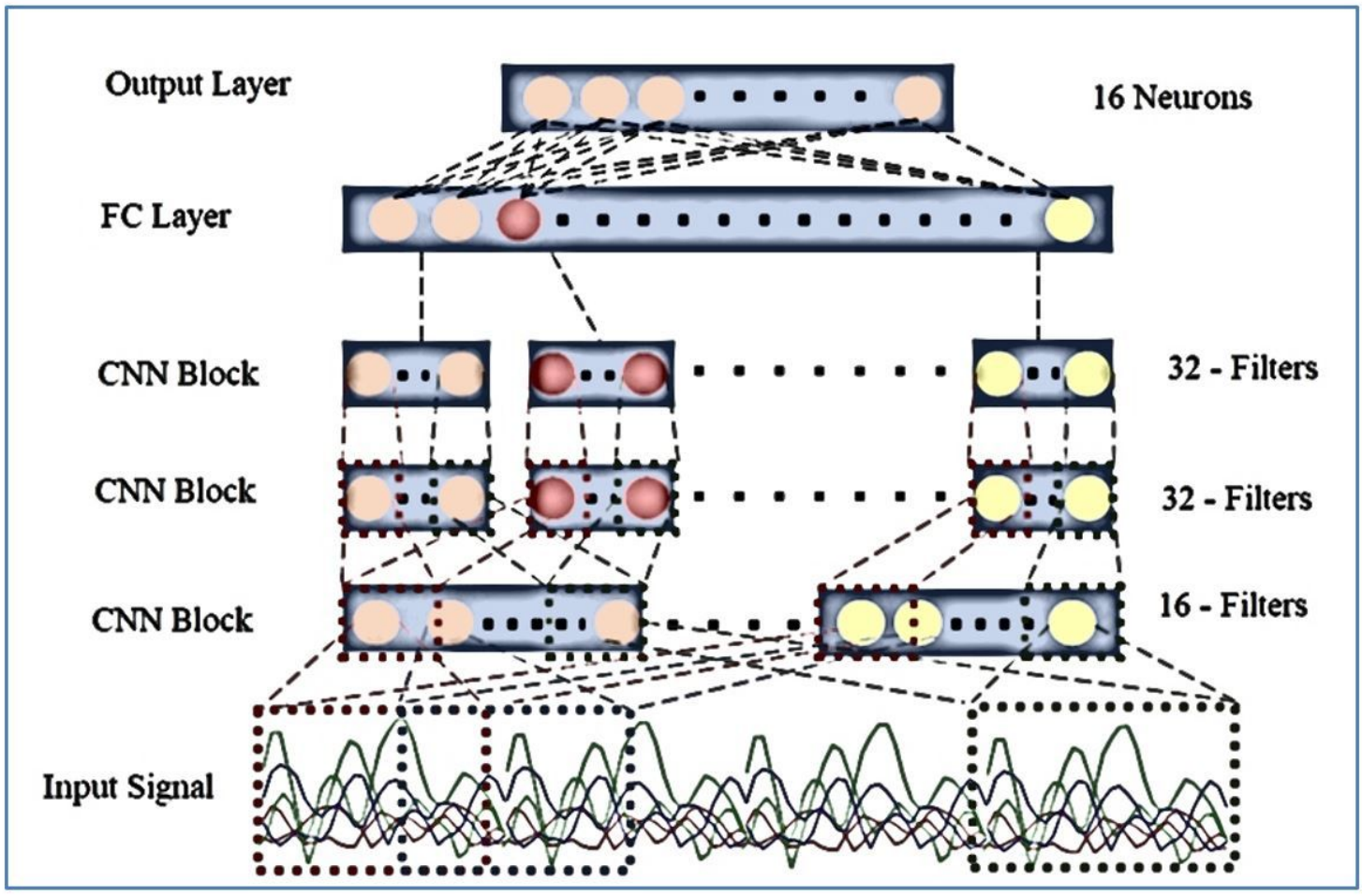

Figure 4

Basic Deep Learning Structure

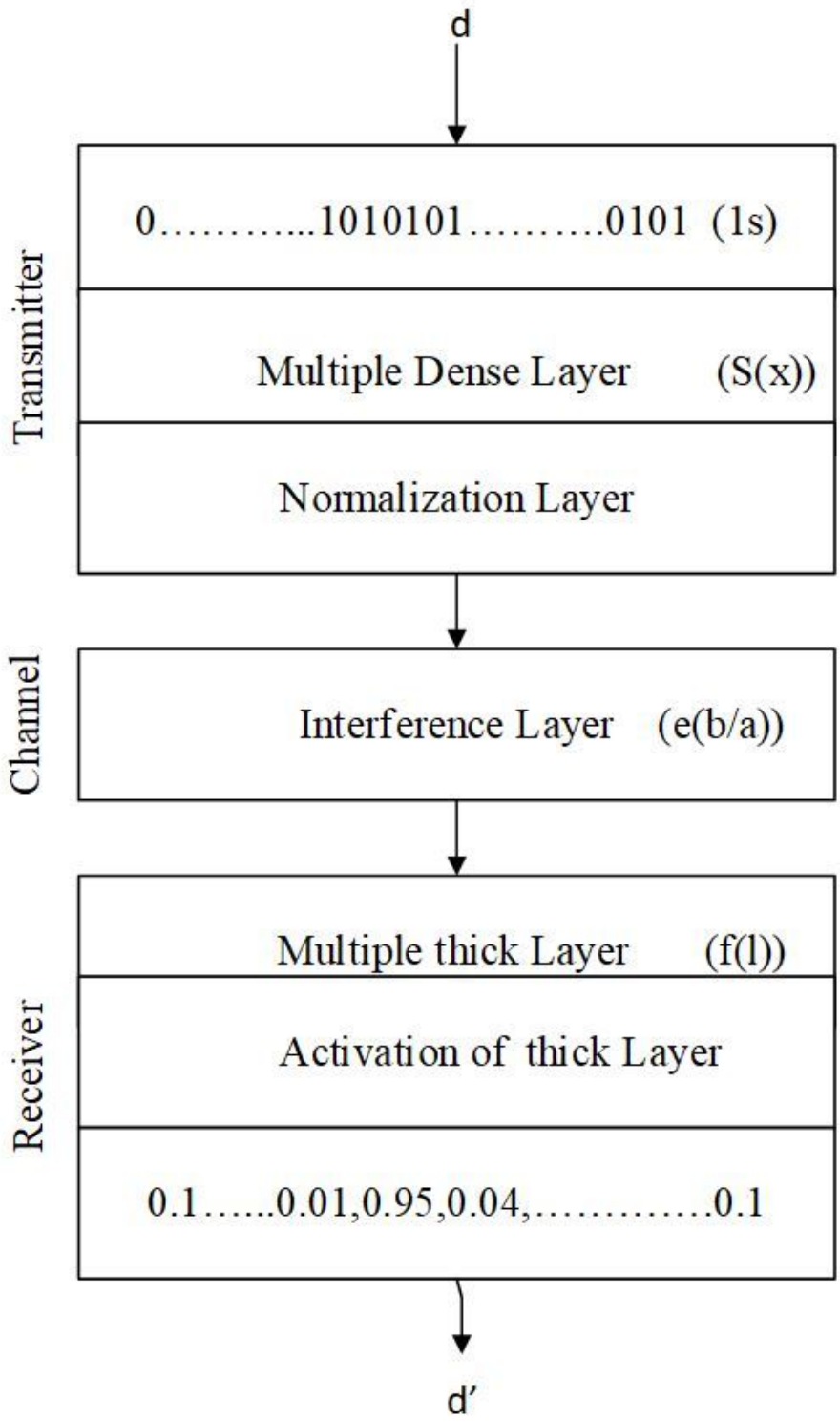

Figure 5

Single Input Single Output in data encoder

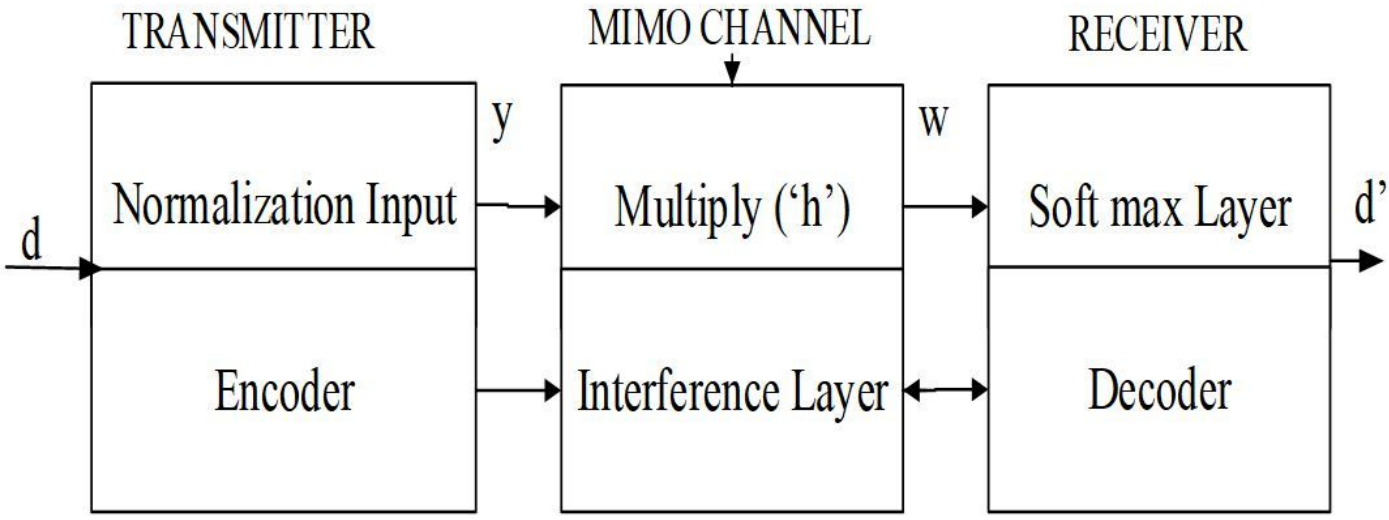

Figure 6

Autoencoder for MIMO Channel

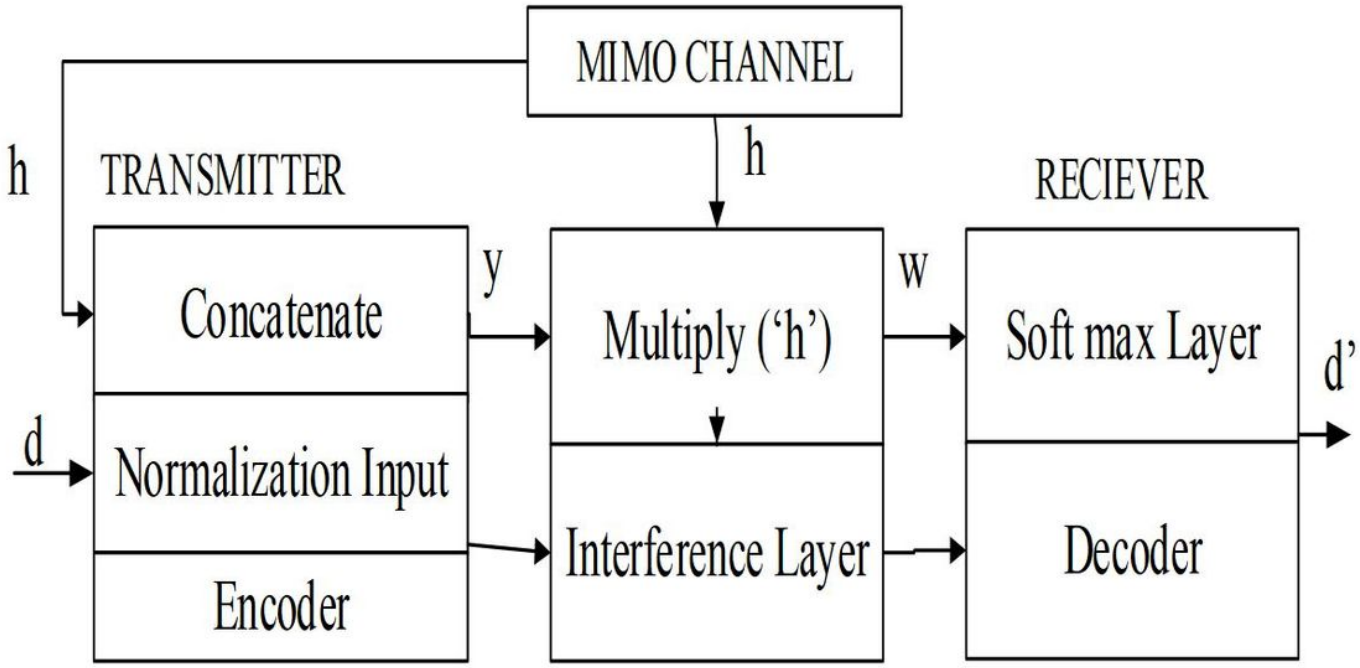

Figure 7

MIMO Channel with Perfect CSI on data encoder

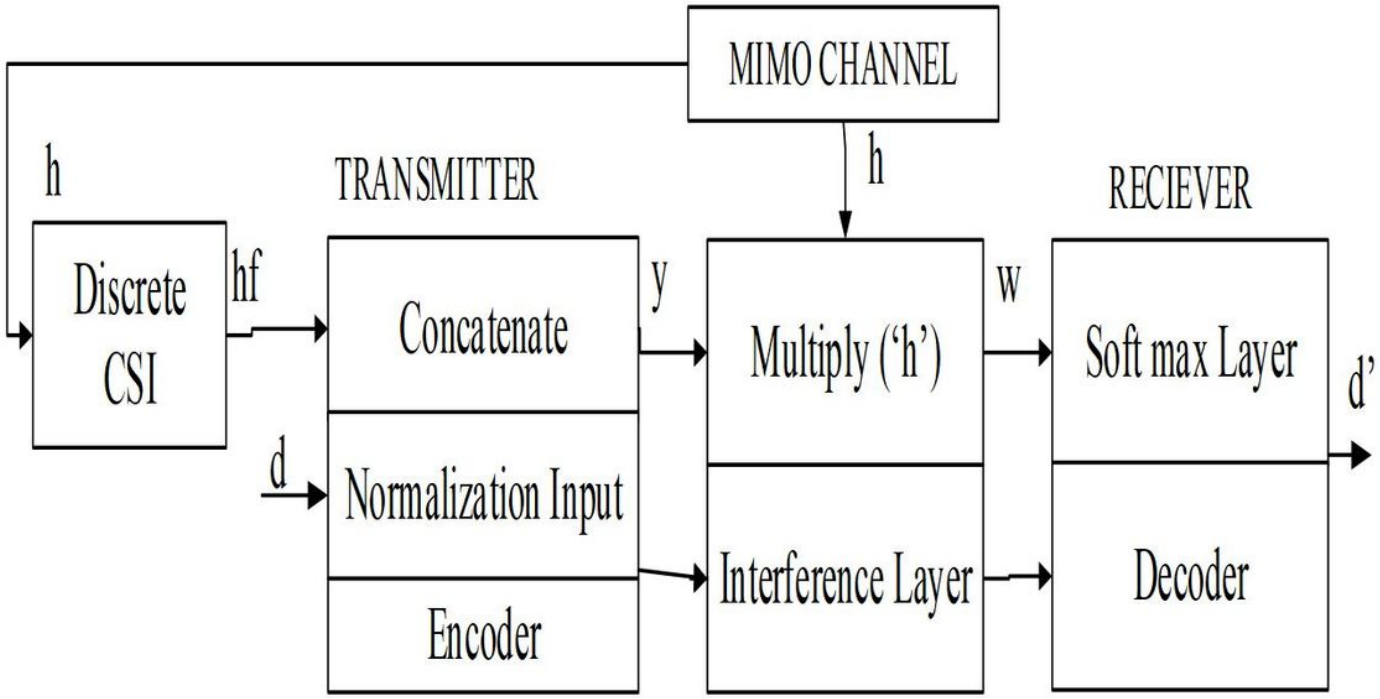

Figure 8

MIMO Channel without CSI on f-Bit Discrete data encoder

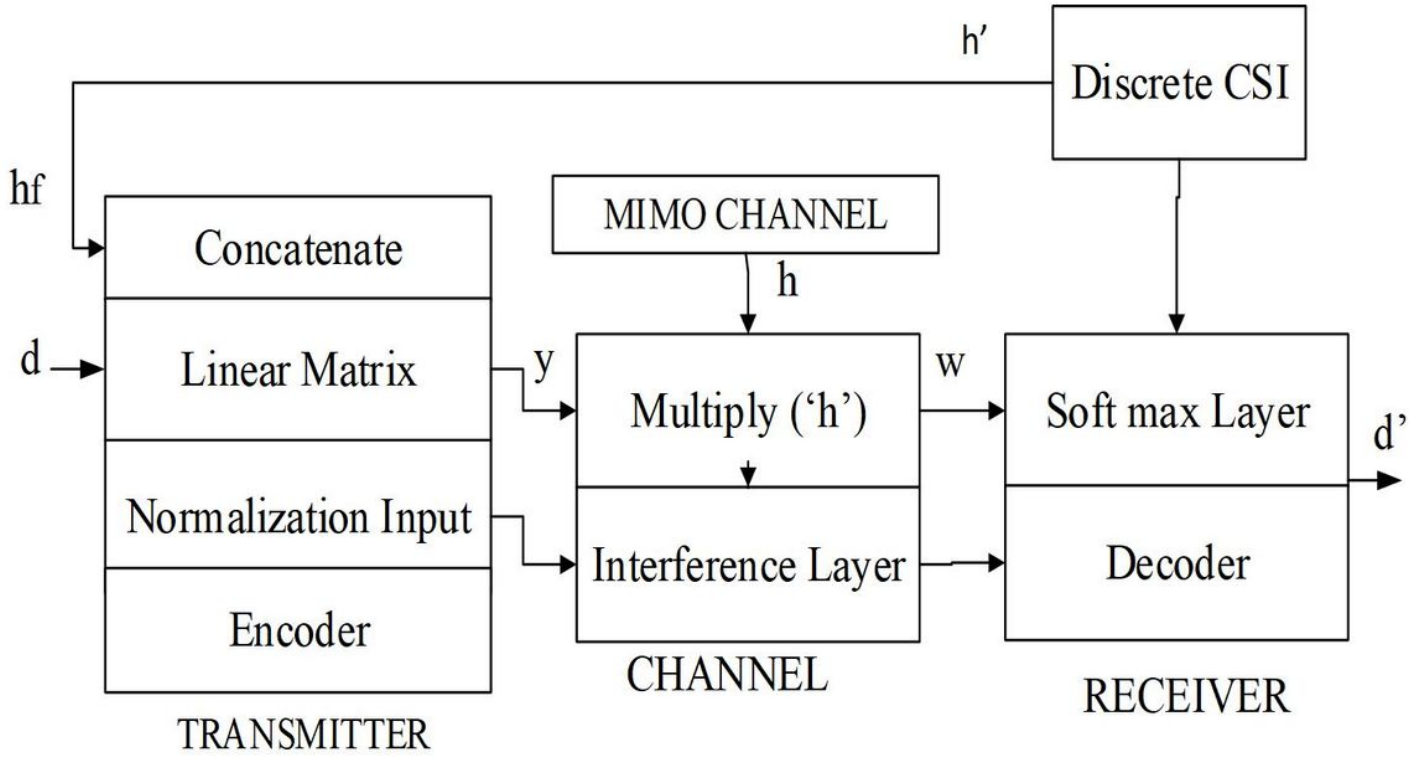

Figure 9

MIMO with t-Bit CSI for Deployment Scheme

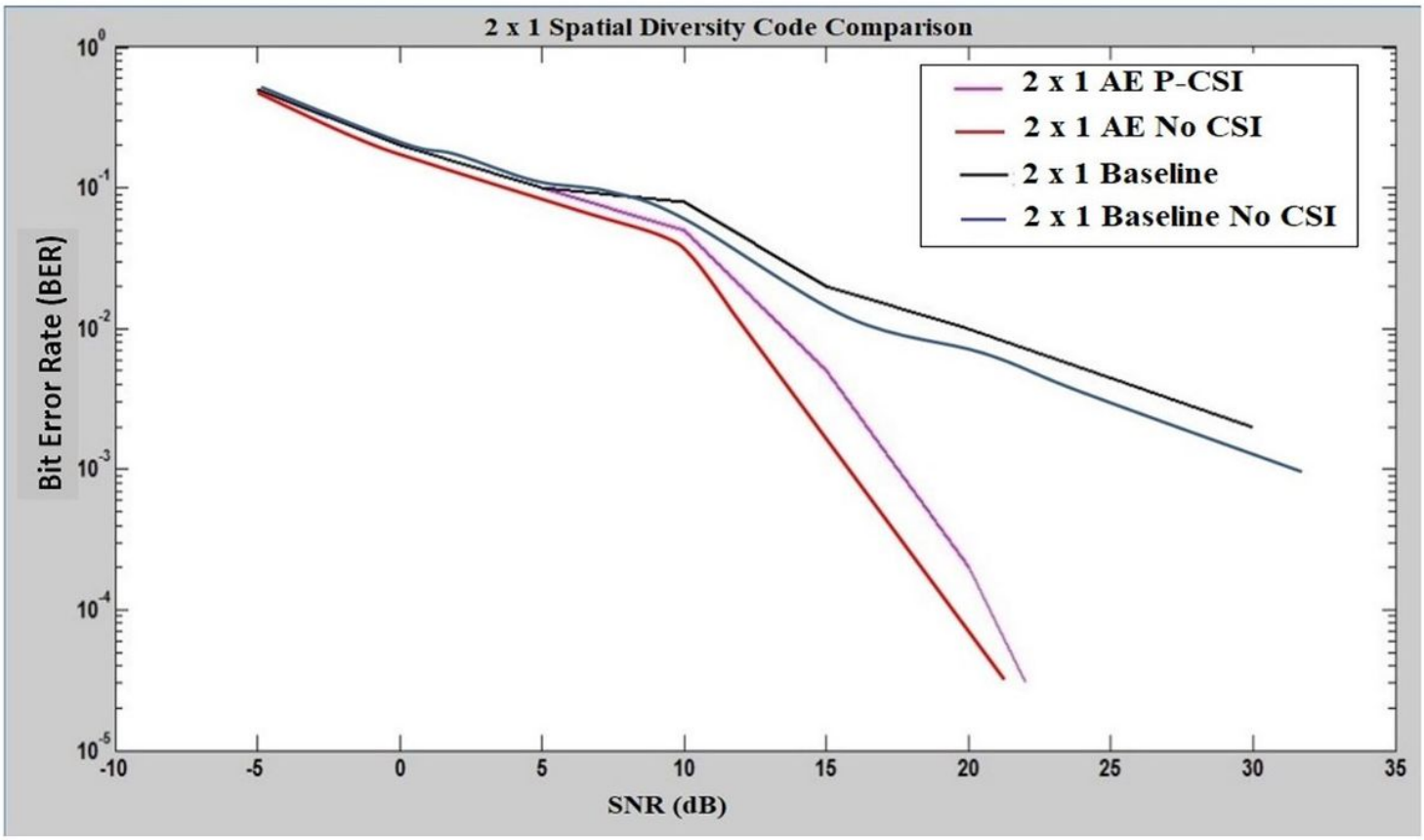

Figure 10

Performance of error rate in Diversity Scheme

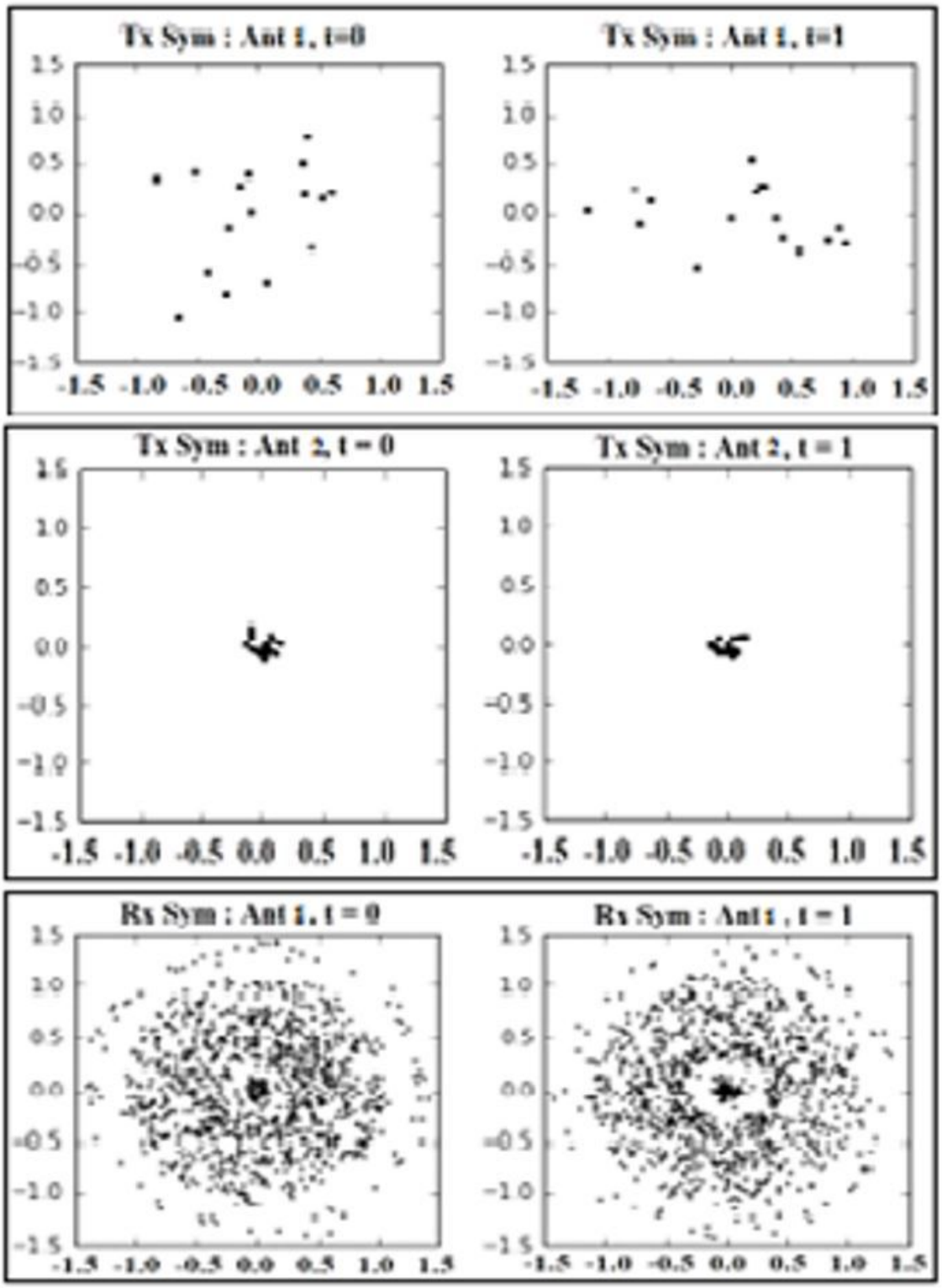

Figure 11

2x1- Random Channels

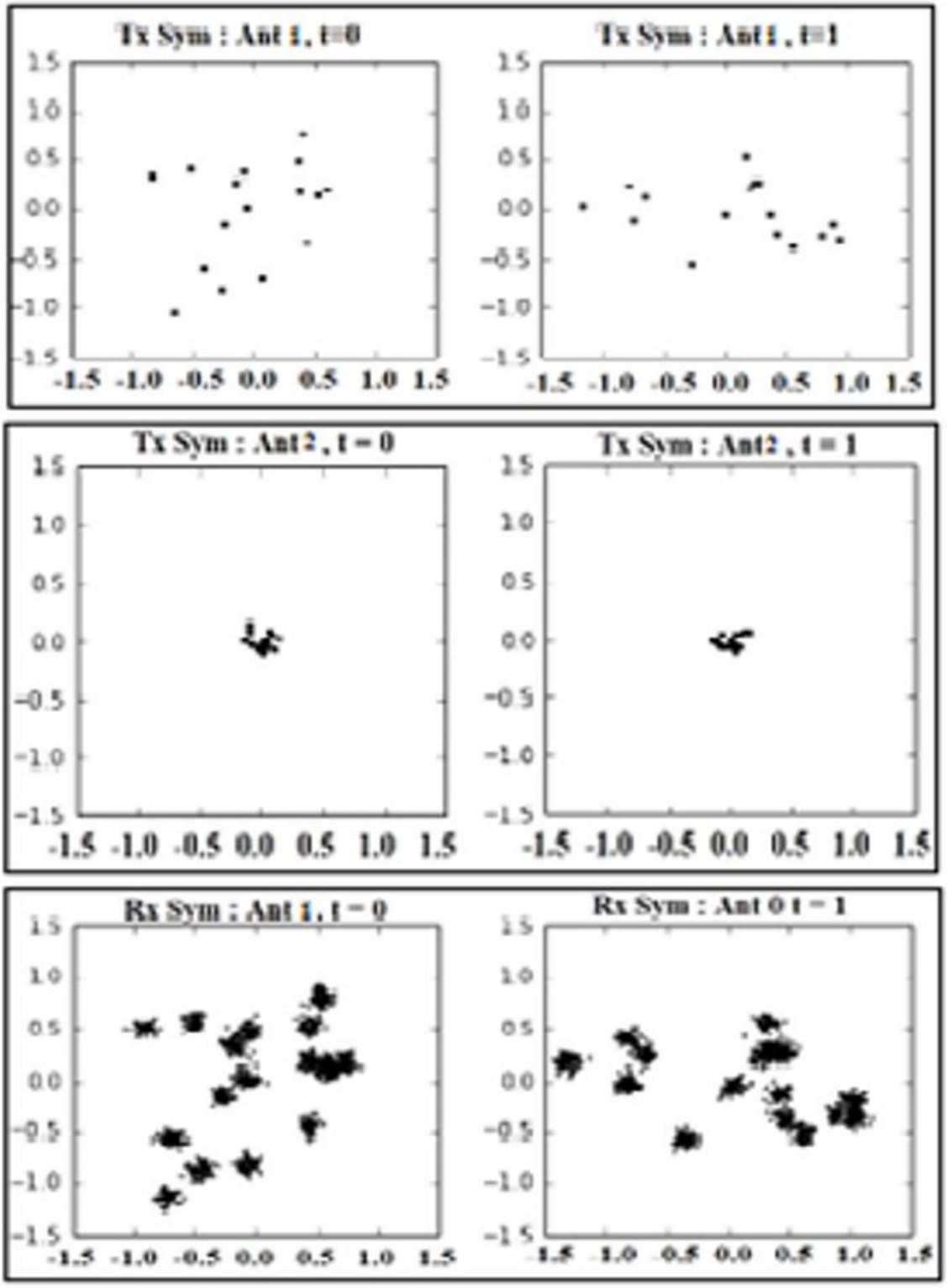

Figure 12

2x1- Diagonal Channel.

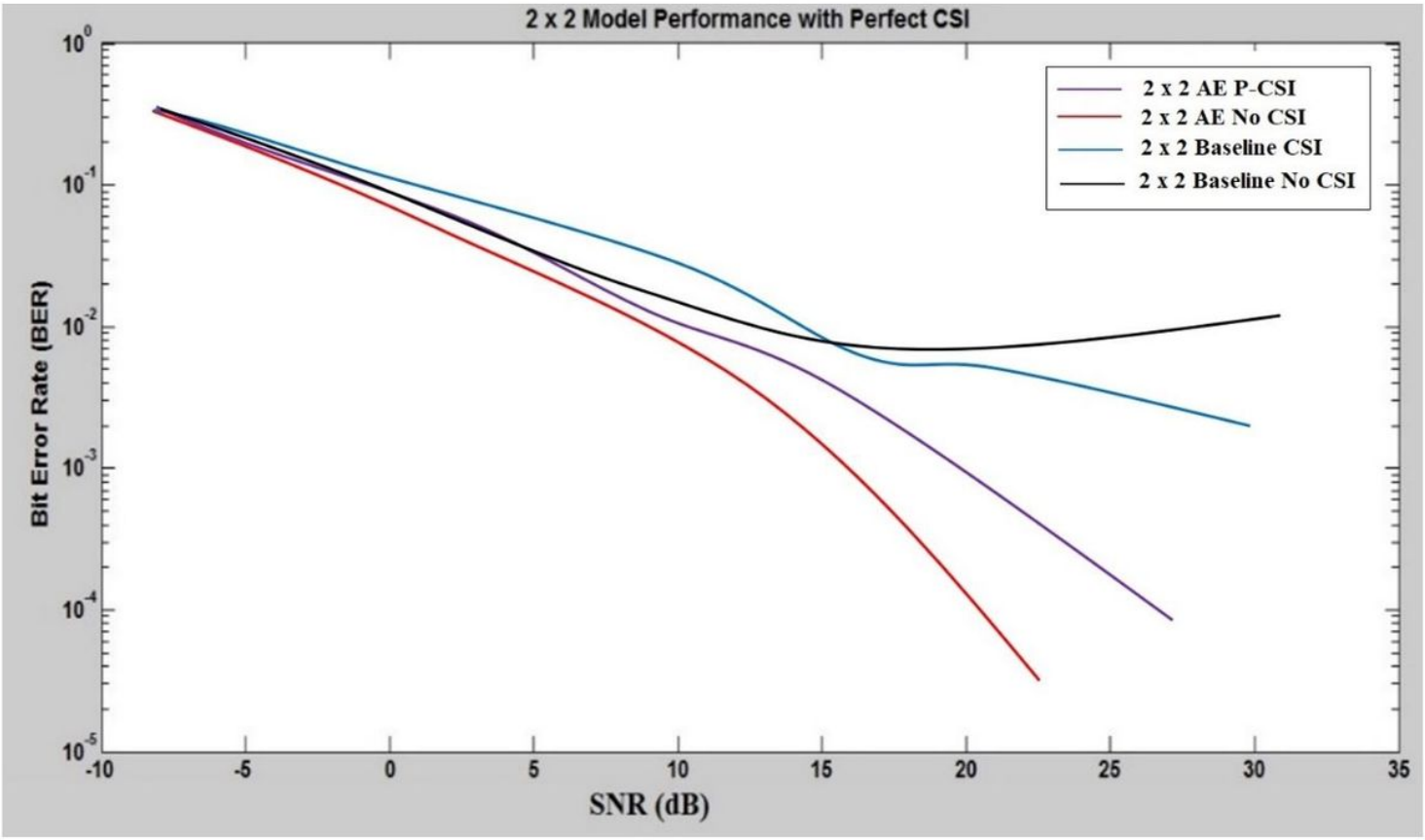

Figure 13

Error Rate Performance of perfect CSI in 2x2 Scheme

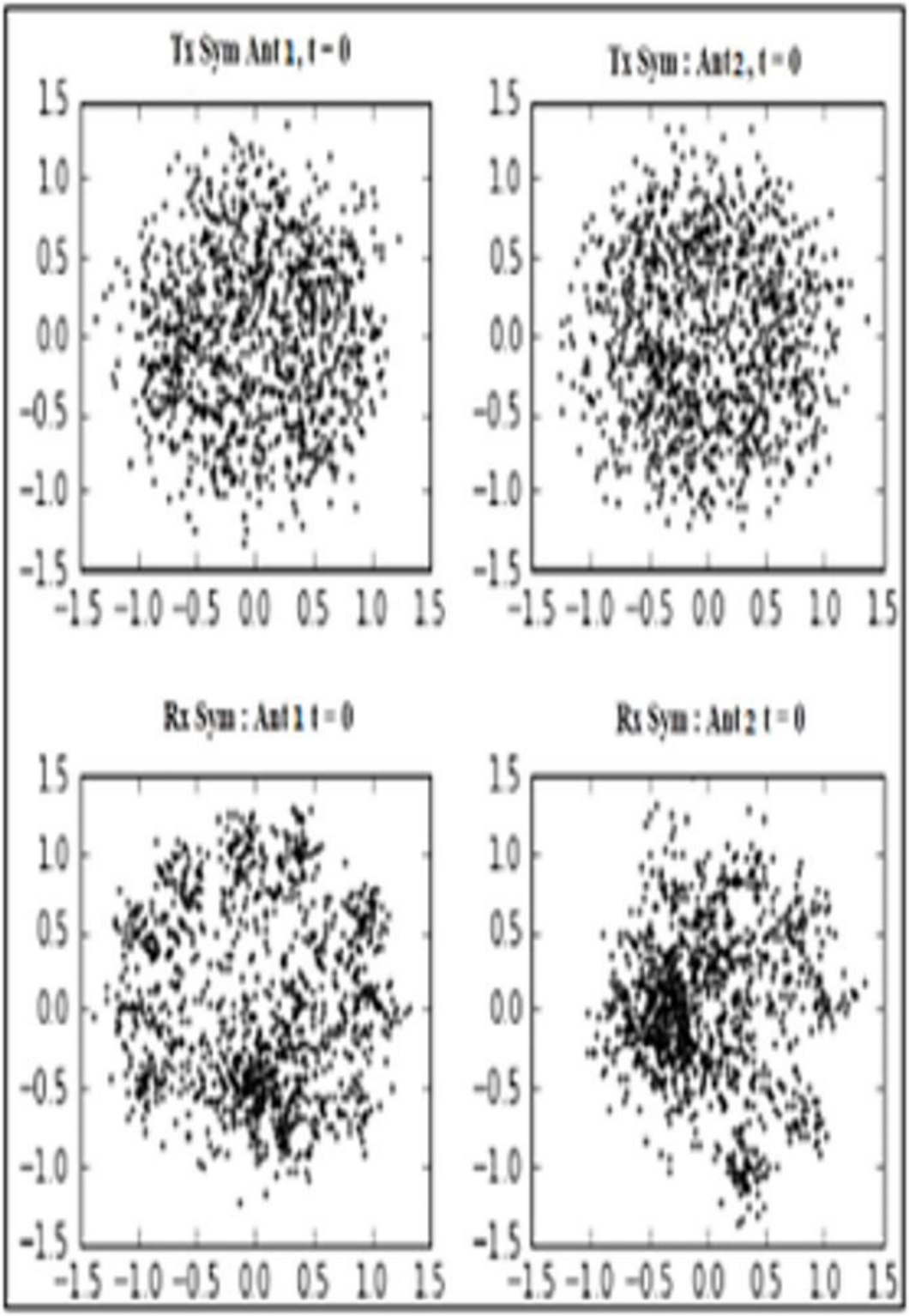

Figure 14

2x2 - Random Channels.

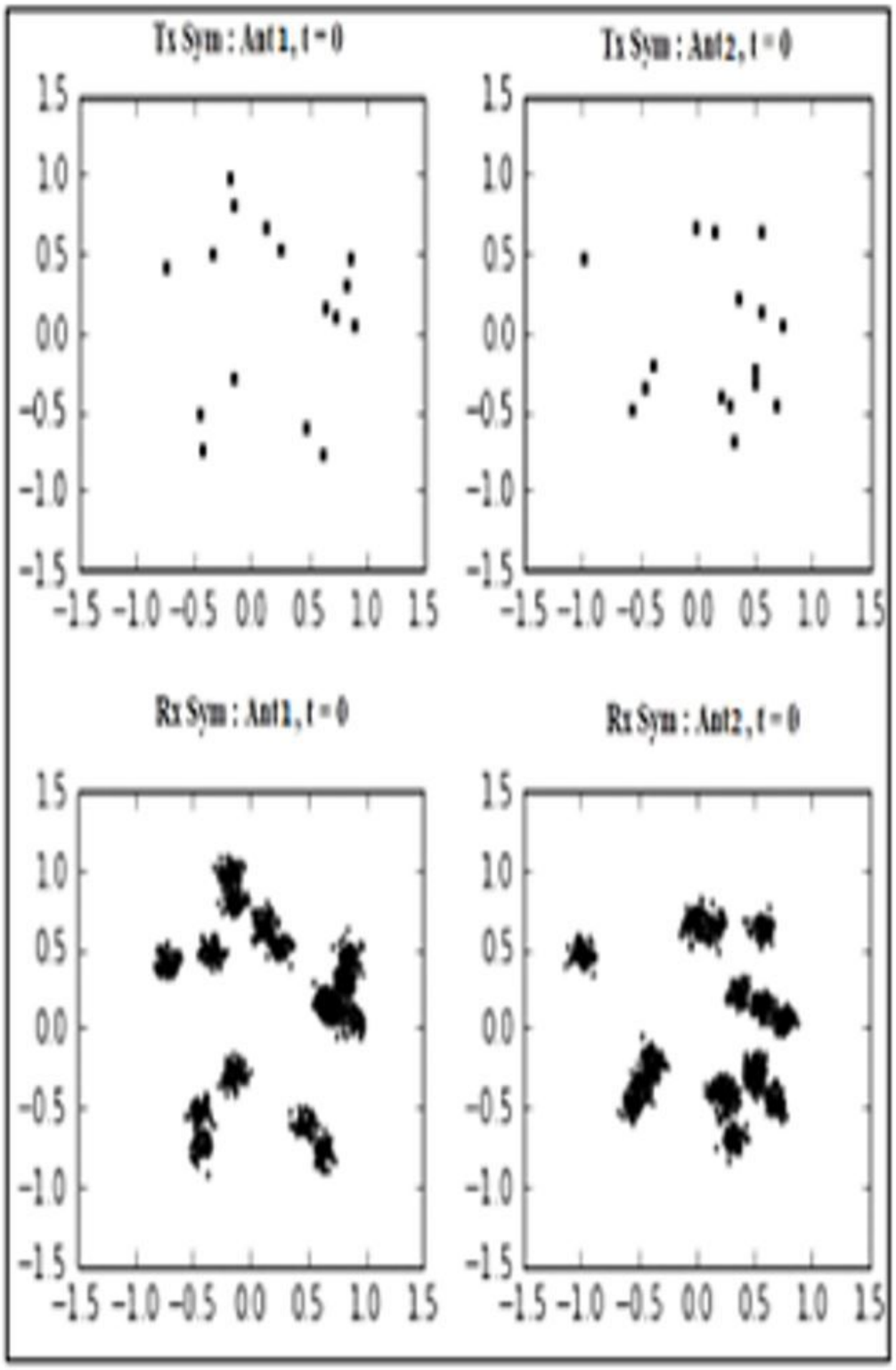

Figure 15

2x2 - Diagonal Channel.

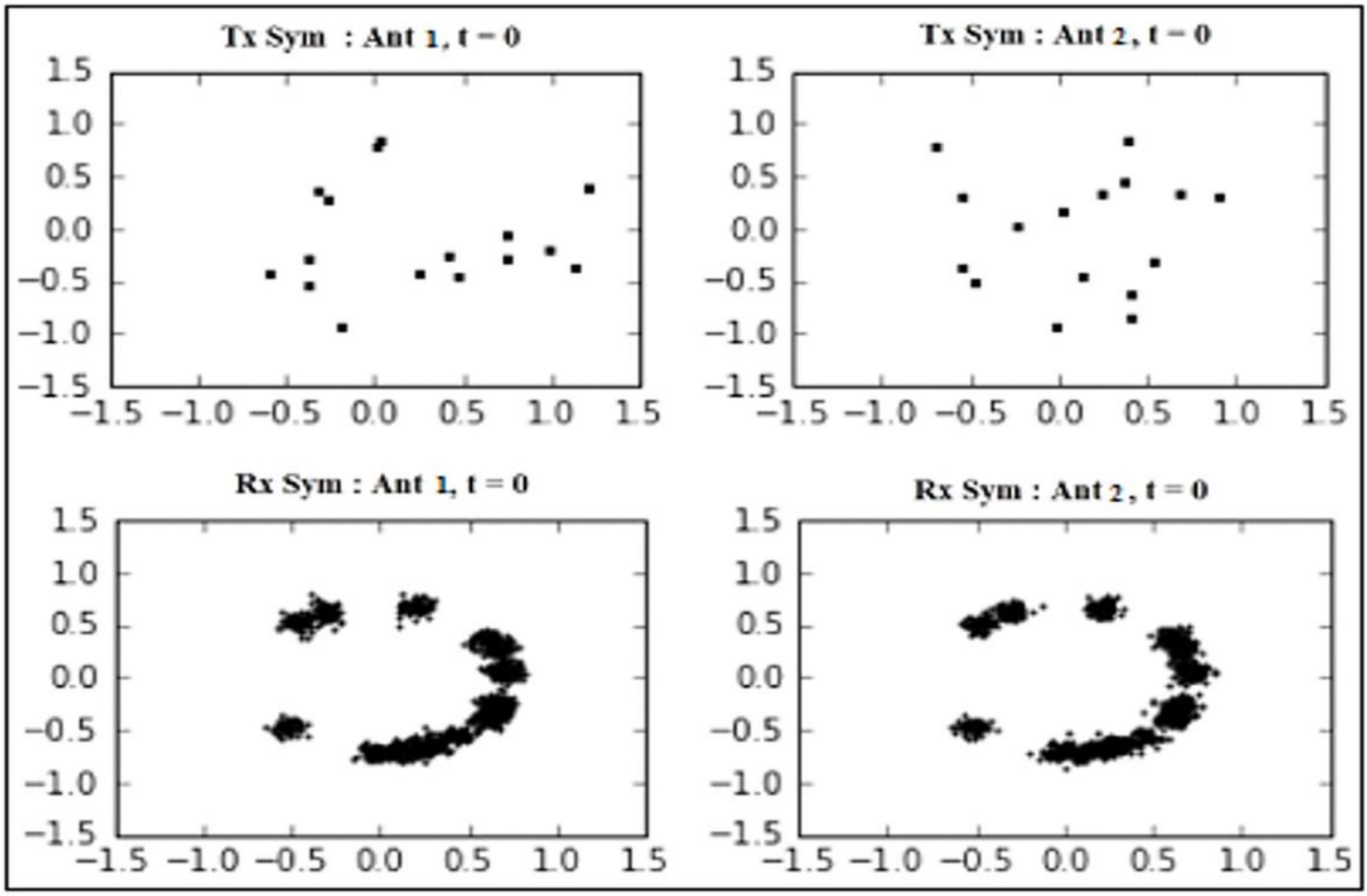

Figure 16

All Single Channel with 2x2 Scheme

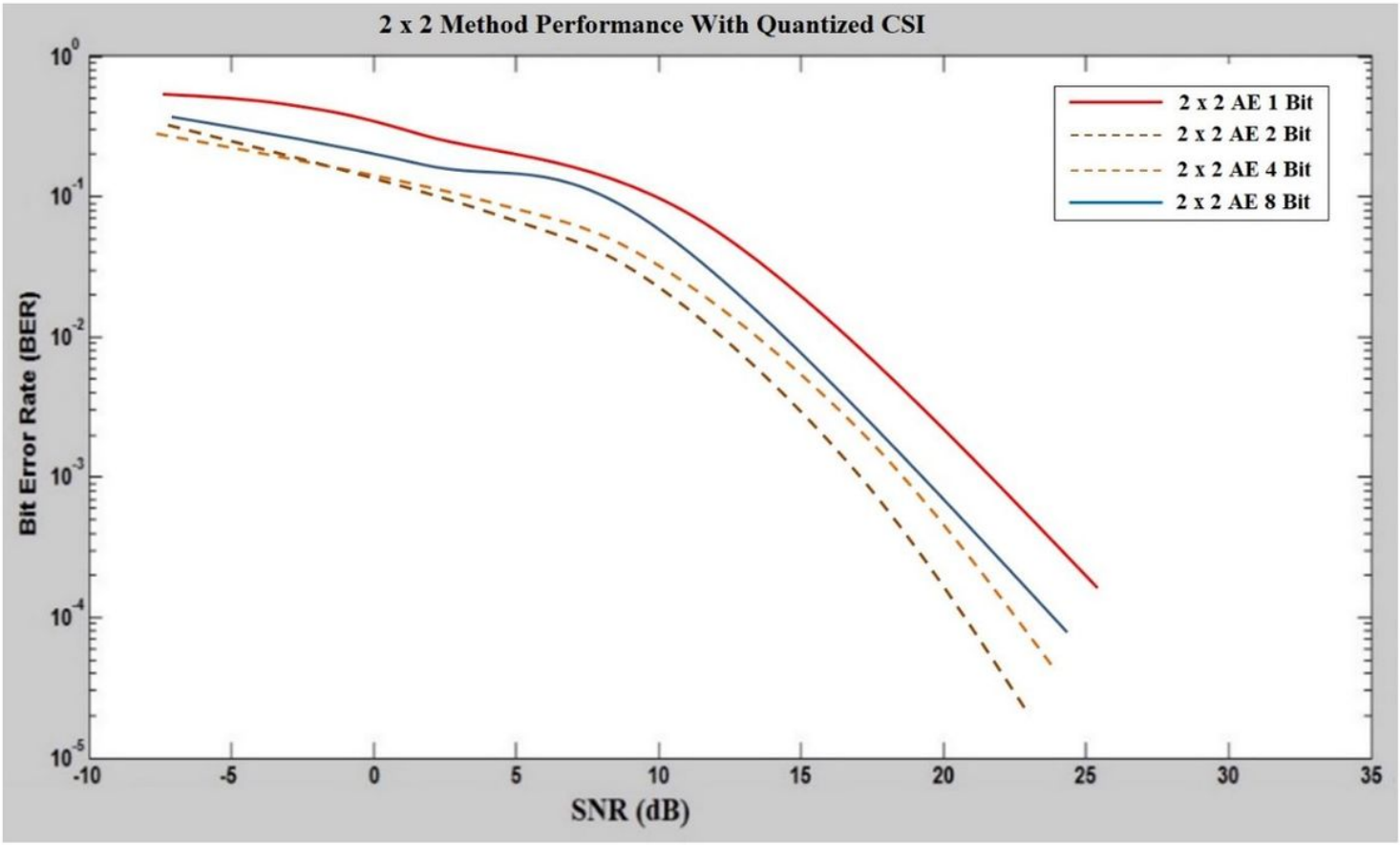

Figure 17

Error Rate Performance of Baseline 2x2 Scheme (Quantized CSI).